Chapter 6
Results and Discussions- Concrete

6.1 Introduction

This chapter examines test results for the mechanical properties, durability, and thermal stability of concrete mixes containing MK and NS, drawing comparisons with normal concrete. Detailed discussions on compressive strength, split tensile strength, and flexural strength outcomes are provided under the mechanical properties section. The study of durability performance, encompassing resistance to carbonation, acid attack, and water absorption rate, is conducted and expounded upon in the relevant segments. The evaluation of thermal resistance, as determined by measuring residual compressive strength after exposure to temperatures up to 800°C, is deliberated upon in the thermal stability section. Furthermore, the chapter delves into concrete's spalling and surface cracking behaviour under high-temperature conditions. Microstructural findings, as analysed through XRD, TGA/DSC, and SEM techniques, are presented and correlated with mechanical and durability test results, offering a comprehensive understanding, including insights into changes in the concrete microstructure under elevated temperatures.

6.2 Mechanical properties

6.2.1 Compressive strength

An extensive examination of the compressive strength of various concrete mixes at their different curing ages of 3, 7, 14, 28, 56, 90, and 180 days is presented in this section. The results are systematically compared with the compressive strength exhibited by reference concrete. The session provides valuable insights into the progressive development of

strength in concrete mixtures at different curing periods. Figure 6.1 illustrates the compressive strength of the various concrete compositions at different curing periods.

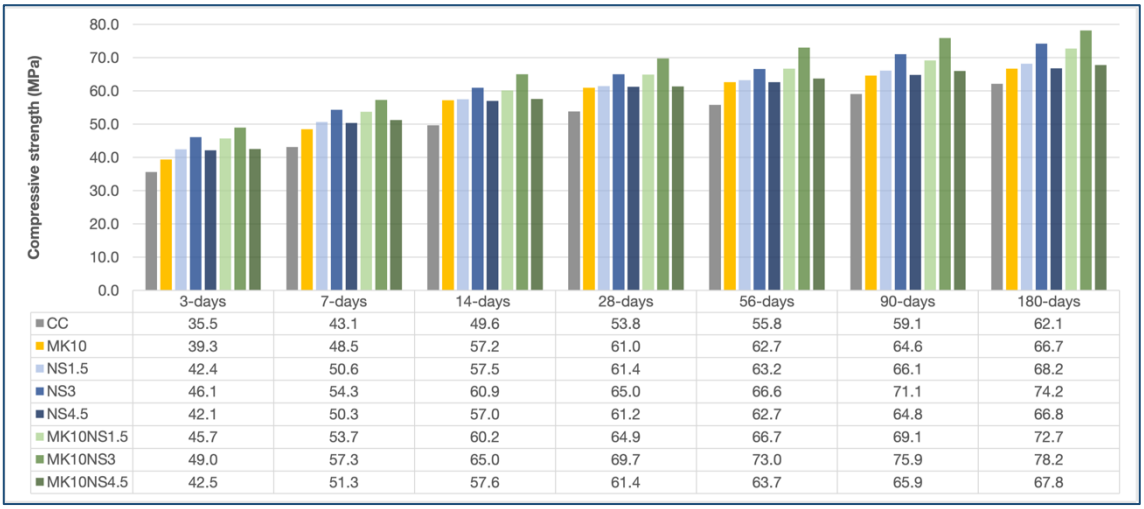

	3-days	7-days	14-days	28-days	56-days	90-days	180-days
CC	35.5	43.1	49.6	53.8	55.8	59.1	62.1
MK10	39.3	48.5	57.2	61.0	62.7	64.6	66.7
NS1.5	42.4	50.6	57.5	61.4	63.2	66.1	68.2
NS3	46.1	54.3	60.9	65.0	66.6	71.1	74.2
NS4.5	42.1	50.3	57.0	61.2	62.7	64.8	66.8
MK10NS1.5	45.7	53.7	60.2	64.9	66.7	69.1	72.7
MK10NS3	49.0	57.3	65.0	69.7	73.0	75.9	78.2
MK10NS4.5	42.5	51.3	57.6	61.4	63.7	65.9	67.8

Figure 6.1. Compressive strength vs. curing time of concrete samples

Following the initial three days of curing, distinct differences in concrete mixes were observed. The MK10 binary mix exhibited an 11% higher compressive strength compared to the reference mix CC, indicating MK's positive impact on early strength development due to its filler effect and rapid cement hydration acceleration within 24 hours [282]. Similarly, the NS1.5 binary mix showed a 19% improvement in compressive strength over CC, while NS3 demonstrated a notable 29% gain. NS4.5 also displayed significant progress with an 18.6% increase in compressive strength, attributed to the robust pozzolanic reactivity of NS particles, contributing to enhanced early-age compressive strength in NS binary concretes [283]. The ternary mix MK10NS1.5 achieved a 28.4% rise in compressive strength over the CC reference, with MK10NS3 showcasing a remarkable 38% enhancement and MK10NS4.5 demonstrating a notable 19.5% increase in compressive strength, underscoring the synergistic effects of MK and NS in these combinations.

At the 7-day mark, the concrete's strength development continued beyond the initial gains. The MK10 binary mix maintained its lead over CC, showing a 12% increase in compressive strength, confirming the lasting influence of 10% MK. Additionally, NS1.5 and NS3 displayed significant strength enhancements, exceeding the reference mix by around 17.3% and 26%, respectively. NS4.5 achieved a 16.7% increase over CC. Ternary blends, such as MK10NS1.5 and MK10NS3, outperformed CC by 25% and 33% at 7 days, demonstrating the synergistic effects of MK and NS and their impact on enhancing concrete strength. The 14-day compressive strength results provided insights into the intermediate strength progression of concrete mixtures, with MK10 maintaining a 16% compressive strength enhancement over CC, highlighting the positive influence of 10% MK content. NS-containing mixes like NS1.5, NS3, and NS4.5 showed significant improvements, with NS3 surpassing CC by approximately 23%, while ternary blends, especially MK10NS3, consistently exhibited strength enhancement, achieving a 31% increase compared to CC [284].

The 28-day compressive strength evaluation plays a crucial role in assessing concrete's maturity and structural suitability. At this milestone, the reference mix, CC, achieved a compressive strength of 53.8 MPa, while the MK10 binary mix maintained its strength advantage, reaching 61 MPa at 28 days, representing a 13% increase over CC. This strength enhancement in the MK10 mix can be attributed to various factors, such as the filler effect, accelerated cement hydration, and pozzolanic reactions. MK's role in enhancing concrete density and strength lies in accelerating alite hydration and pozzolanic reaction kinetics, optimising microstructure packing through void filling, and improving bonding and solid volume, consequently increasing compressive strength [284,287].

Among the NS binary mixes, NS1.5 showed a 14% increase in strength over CC, while NS3 exhibited the highest compressive strength of 65 MPa, surpassing CC by 21%. However, NS4.5 did not significantly improve strength over NS3, potentially due to particle agglomeration at higher concentrations, resulting in non-uniform dispersion and weaker zones [286].

Ternary mixes at 28 days, particularly MK10NS1.5 and MK10NS3, outperformed binary combinations, with MK10NS1.5 achieving a compressive strength of 64.9 MPa, a 20.7% increase over CC, and MK10NS3 showcasing a remarkable 30% improvement, reaching a compressive strength of 69.7 MPa. The superior strength of MK10NS3 can be attributed to the efficient synergy between 10% MK and 3% NS particles, leveraging their distinct mechanisms to significantly contribute to overall strength development. The positive impact of MK and NS interaction is further highlighted by their continued strength enhancement, as seen in MK10NS3, where the proportion of unreacted MK was relatively low, allowing for the full manifestation of NS's pozzolanic and structural effects. Conversely, the MK10NS4.5 mixture exhibited a compressive strength of 61.4 MPa, a 14.1% increase over CC, indicating that NS concentrations above 3% may inhibit strength due to particle agglomeration, reduced CH availability, and potentially decreased hydration rates and CSH gel formation [282,287,288].

The 56-day compressive strength assessment highlighted the enduring strength performance of the concrete mixes. MK10 maintained its strength superiority over CC, showing a significant 12% increase in compressive strength, underscoring the lasting advantages of MK even in later curing stages. Similarly, the NS1.5 binary mix continued to outperform CC with a 13% increase in compressive strength, while 3% NS achieved a

substantial 19% compressive strength increase, reaching 66.6 MPa in its binary concrete, and NS4.5 exhibited a 12% compressive strength increase compared to CC. Ternary blends such as MK10NS1.5, MK10NS3, and MK10NS4.5 showcased notable compressive strength increments of 19.5%, 30.9%, and 14.1%, respectively, compared to CC, indicating consistent long-term strength development and emphasising the synergistic effects, especially evident in MK10NS3. At 56 days, MK10NS3 showed a higher percentage increase in compressive strength compared to 28 days concerning CC, while MK10NS4.5 maintained a consistent 14% increase in compressive strength compared to the earlier period.

Moving to the 90-day compressive strength results, further insights into the concrete's performance under extended curing conditions were gained. MK10 sustained its strength advantage over CC with a 10% increase in compressive strength, highlighting its extended pozzolanic activity. Among the NS blends, NS3 exhibited the highest strength improvement of approximately 20% over CC, while NS1.5 and NS4.5 showed increases of about 12% and 10%, respectively. Ternary mixes like MK10NS1.5, MK10NS3, and MK10NS4.5 also demonstrated enhanced compressive strength after 90 days, with MK10NS3 reporting the highest compressive strength at 75.9 MPa, marking a significant 28.5% increase over CC. MK10NS1.5 and MK10NS4.5 showed increases of 17% and approximately 12%, respectively, compared to CC. Lastly, the 180-day compressive strength test delved deeper into the concrete's long-term performance in compressive strength, with binary concrete MK10 showing a 7.4% increase compared to the reference mix. The NS binary blends showed progressive compressive strength enhancements, with NS3 displaying the highest improvement of 19.4% over CC, while NS1.5 and NS4.5 exhibited increments of 9.7% and 7.5%, respectively. However, the ternary concrete mixes, benefiting from the synergistic effect of MK and NS, exhibited the most significant

strength development, with MK10NS1.5 reporting a 17% increase in compressive strength compared to the reference and MK10NS3 displaying a substantial strength increment of approximately 26%. Despite a more modest increase of 9%, MK10NS4.5 outperformed its binary counterparts.

The 180-day compressive strength test provides a deeper insight into concrete's long-term performance in compressive strength. The binary concrete MK10 showed a 7.4% increase compared to reference concrete. NS binary blends demonstrated progressive compressive strength enhancements, with NS3 displaying the highest improvement of 19.4% compared to CC, while NS1.5 and NS4.5 showed increments of 9.7% and 7.5%, respectively. However, ternary concrete, benefiting from the synergistic effect of MK and NS, exhibited the highest strength development. MK10NS1.5 reported a 17% increase in compressive strength compared to the reference concrete, while MK10NS3 displayed a significant strength increment of approximately 26%. Despite a more modest increase of 9%, MK10NS4.5 outperformed its binary counterparts.

The incorporation of MK played a significant role in increasing the compressive strength of the concrete due to its high surface area, which surpasses that of cement by 100 times, providing ample pozzolanic active sites for reacting with CH to generate additional CSH and CASH [240–243]. The fine particles of MK effectively filled the gaps between cement particles, resulting in a denser and less porous microstructure, ultimately enhancing the overall strength properties. On the other hand, NS with its extensive surface area of 150 m^2/g and small average diameter of 18.1 nm, exhibited a higher concentration in the cement-water mix compared to MK, consequently introducing a significantly larger surface area of active pozzolan compared to MK. In the 1.5 to 3% range of NS, a

substantial portion actively contributes to the pozzolanic reaction, thereby increasing the CSH volume and, consequently, the compressive strength in the concrete. However, elevated doses of pozzolanic materials such as NS may not proportionally boost the hydration rate due to the absence of crystalline CH necessary for forming secondary CSH gel [235]. The decline in strength at higher NS dosages can be attributed to two possible factors; firstly, if the cement hydration rate is inadequate to promote a pozzolanic reaction on the highly reactive NS surfaces at higher concentrations, unreacted NS particles might remain in the concrete. Secondly, agglomeration of NS particles at elevated doses could lead to uneven dispersion in the concrete, impacting the pozzolanic reaction and reducing strength. Despite the absence of unreacted NS particles noted in morphological studies, the reduction in strength at a 4.5% NS dosage is likely due to particle agglomeration.

Moreover, the compressive strength of ternary concrete incorporating 10% MK and 1.5 to 3% NS exceeded that of their binary counterparts, thanks to the synergistic effects observed. MK, with its extensive surface area, provided abundant pozzolanic sites for reacting with CH, yielding additional CSH and CASH and contributing to the enhanced density of the microstructure. Meanwhile, NS, with its larger surface area, introduced a more active pozzolan even at lower concentrations, thereby boosting the strength of the concrete. The collaboration between MK and NS optimised particle packing, promoting a highly dense and less porous concrete structure, collectively leading to improved mechanical properties of the concrete.

6.2.2 Split tensile strength

Concrete is not inherently capable of withstanding direct tension. However, the split tensile test can determine the load at which concrete may develop cracks.

The split tensile strength of all mixes exceeded the JSCE-2007 value,

$$f_{spt} = 0.23 f_c^{0.67}$$ Equation 6.1

Where f_{spt} and f_c are the split tensile strength and characteristic compressive strength respectively in MPa.

Figure 6.2 compares the obtained split tensile strength values and the JSCE-2007 [289] benchmarks. The results indicate that except for NS4.5 and MK10NS4.5 mixes, the split tensile strength values for the various concrete blends exceeded those of the normal concrete mix. The difference in split tensile strength between CC and MK10 concrete was negligible. Furthermore, it was observed that the split tensile strength increased with the incorporation of NS dosage up to 3%, after which it decreased in both binary and ternary mixes.

In the binary mixes, MK10 exhibited a slightly 2% increase in split tensile strength than CC. The NS1.5 and NS3 exhibited 1.3% and 10.5% higher split tensile strength, respectively, while NS4.5 showed a 4.7% decrease.

Among the blends, the MK10NS3 mix demonstrated the highest split tensile strength with 4.38 MPa, followed closely by MK10NS1.5, which achieved a value of 4.15 MPa. These values represent a significant enhancement compared to CC, with 15.6% and 9.5% improvements, respectively and can be attributed to the reduction in pore volume and the formation of a denser and stronger interfacial transition zone (ITZ), as both MK and NS can densify the ITZ [96–98,195].

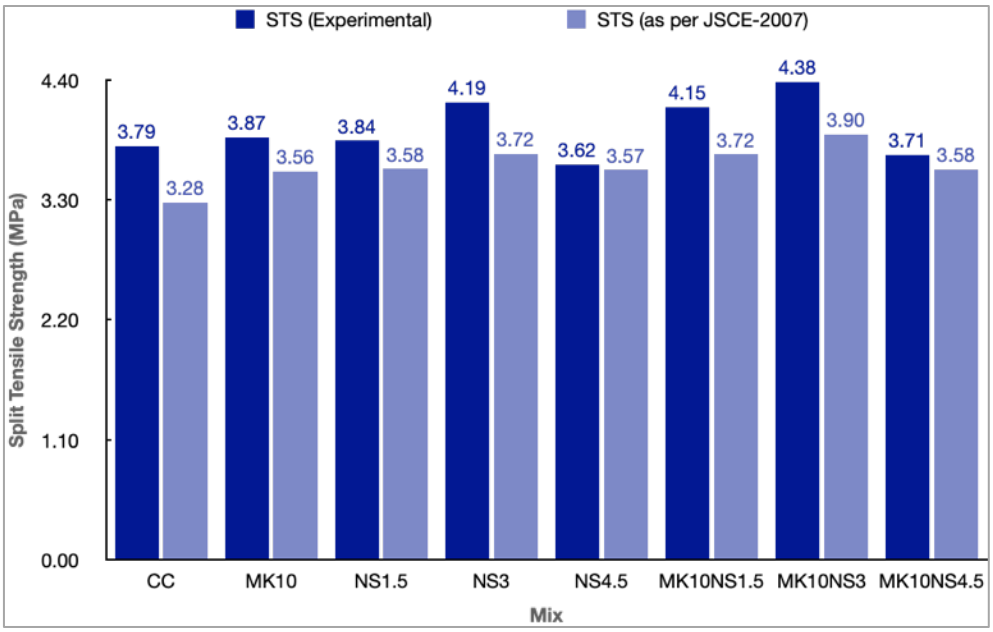

Figure 6.2 Comparison of split tensile strength with JSCE-2007 benchmark

6.2.3 Flexural strength

Figure 6.3 provides a visual representation of the flexural strength observed in the concrete mixes alongside the flexural strength derived from the empirical relationship between compressive strength and flexural strength as outlined in IS: 456-2000 [IS 456] [290]. The flexural strength values f_{cr} according to IS standards are determined through the following expression.

$$f_{cr} = 0.7 f_{ck}^{0.5} \qquad \text{Equation 6.2}$$

Where f_{ck} is the characteristic cube compressive strength in MPa.

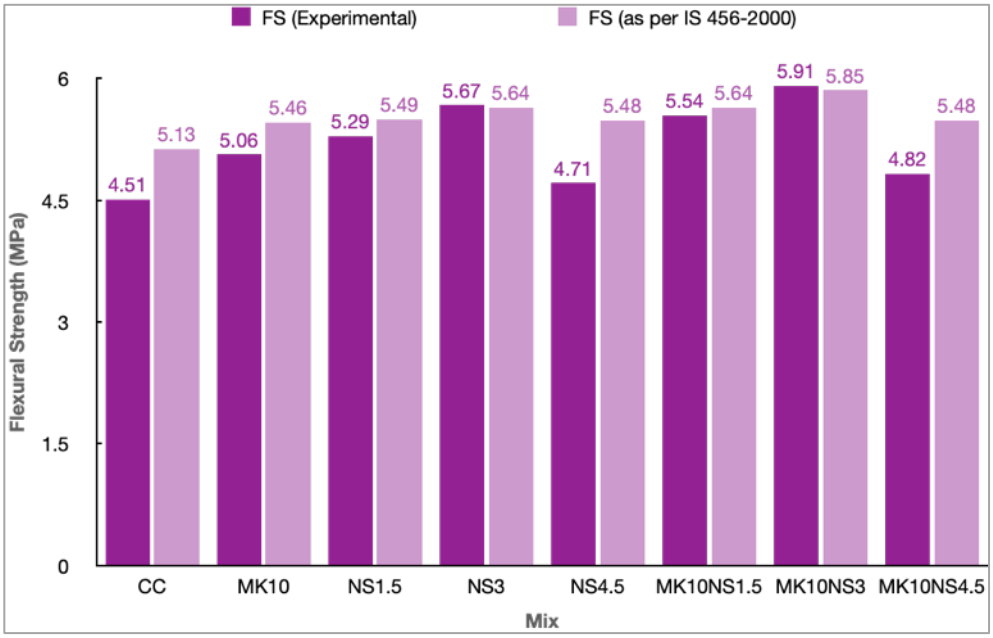

Figure 6.3 Comparison of flexural strength with IS 456-2000 values

The microstructure of the ITZ plays a crucial role in concrete flexural strength. Concrete containing MK and NS exhibited higher flexural strength than normal concrete, indicating densification and strengthening of the ITZ due to NS and MK. The MK10 mix demonstrated a 6.5% increase in flexural strength compared to CC. Both binary and ternary concrete mixes showed increased flexural strength with NS up to 3%. However, at 4.5% NS, there was a reduction in flexural strength, though it still surpassed that of CC.

In the binary mixes, NS1.5 and NS3 exhibited 17.3% and 25.2% higher flexural strength than CC, respectively, while NS4.5 showed a 4.4% increase. The ternary mix MK10NS3 had the highest flexural strength, surpassing CC by 31%. Additionally, MK10NS1.5 and MK10NS4.5 exhibited flexural strengths of 22.8% and 6.9% higher than CC. It was noted that, except for NS3 and MK10NS3, all mixes had flexural strengths below those predicted by the empirical formula of IS456-2000. Nonetheless, the results underscore

that similar to splitting tensile strength, the incorporation of NS and MK led to an improvement in the flexural strength of concrete. This improvement can be attributed to the enhanced adhesion between the cement paste and aggregate [186] particularly notable when an optimal dosage of 3% NS was present.

6.3 Durability parameters

6.3.1 Carbonation

The carbonation depths of the concrete cubes after 14 days and 28 days of carbonation and the corresponding carbonation coefficient are given in Table 6.1. At 70±5% RH and 7.50±0.5% CO_2 concentration at 27±2°°C, the carbonation depth was high in the reference concrete at 14 and 28 days. As the exposure time increased to 28 days, there was an increase of 67% in carbonation depth in the CC cube compared to the cube tested after 14 days of carbonation.

The carbonation depth observed in binary MK10 concrete exhibited a slight reduction compared to CC, showing approximately 10% less after 28 days of exposure to CO_2. This may be attributed to the formation of excess CSH gel due to the pozzolanic activity of MK, which resulted in a more dense microstructure. The binary concrete mix with NS, however, showed more resistance to the carbonation as the observed carbonation depths of NS1.5, NS3, and NS4.5 were 19, 32, and 15% less after 14 days of CO_2 exposure and 18, 28 and 21% less after 28 days of CO_2 exposure respectively, compared to the CC cube. From the results, it's clear that the carbonation depth decreased as the NS percentage increased up to 3% and with the further addition of NS (4.5%), the carbonation depth increased. It can be attributed to the reaction between excess CH and silica nanoparticles to form additional CSH gel, which densified the concrete microstructure with refined

pores [291]. It can also be observed that the inclusion of NS beyond 3% did not make the concrete denser, as observed earlier.

The ternary concrete with 10%MK and NS varying up to 4.5% outperformed the normal concrete and their binary concrete compositions in carbonation. Following 14 and 28 days of accelerated carbonation, the MK10NS1.5 exhibited a notable reduction in carbonation depth, showcasing values of 33% and 30% lower than those observed in the normal concrete. Demonstrating higher resistance to carbonation, the MK10NS3 mix exhibited a remarkable 38% and 35% reduction in carbonation depth compared to the CC after 14 and 28 days of carbonation, respectively. This heightened resistance can be ascribed to the synergistic influence of MK and NS, contributing to a significantly densified microstructure and resulting in a finely refined pore structure within the matrix. Similarly, the MK10NS4.5 concrete mix displayed enhanced carbonation resistance, revealing a reduction in carbonation depth of 25% and 19% when contrasted with CC after 14 and 28 days of CO_2 exposure. This further underscores the effectiveness of the combined effect of MK and NS in fortifying the concrete's resistance against carbonation.

The carbonation depth depends on the amount of water absorbed by the concrete. Therefore, the porosity of the cover concrete plays a vital role in the carbonation of the concrete. Thus, carbonation is directly correlated to the initial water absorption by the concrete [298], and the CO_2 diffusivity is the function of pore size distribution, total porosity and the degree of saturation by water [293]. From this point of view, it is clear that the pore volumes were reduced, and the pore structure became finer in the ternary concrete due to the combined effect of MK and NS. The concrete samples carbonated

after 14 and 28 days of CO_2 exposure and sprayed with phenolphthalein solution are shown in Figure 6.4

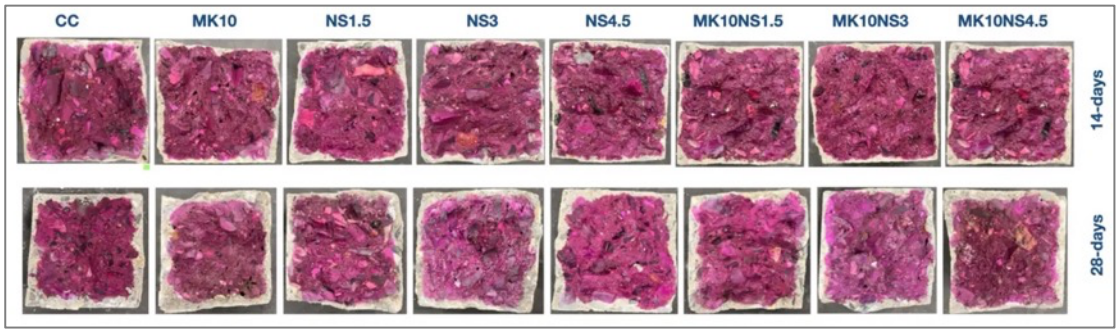

Figure 6.4 Concrete samples treated with phenolphthalein solution

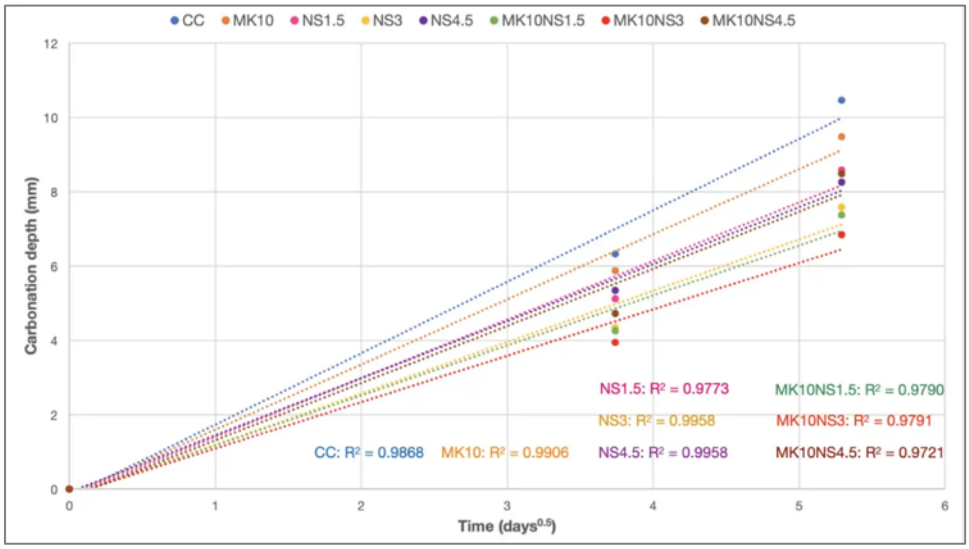

Figure 6.5 Correlation between carbonation depth of concrete mixes and the square root of time

Figure 6.5 illustrates the correlation between the carbonation depth obtained from the phenolphthalein indicator for each concrete mix and the square root of time (14 and 28 days). The slope of the linear regression line indicates the concrete's carbonation

coefficient, k_{acc}. The calculation of k_{acc} adheres to Fick's law of diffusion for the steady-state condition, i.e., constant carbonation coefficient, given below [294].

$$X_c(t) = k_{acc}.\sqrt{(t)} \qquad \text{Equation 6.3}$$

Where, Xc (t) depth of carbonation at time (t) in day

The following relationship between the accelerated and natural carbonation coefficients was employed to derive the carbonation rate under natural conditions from accelerated carbonation tests conducted at 7.5% CO_2 [295].

$$\frac{k_{acc}}{k_{nat}} = \frac{\sqrt{ø_{acc}}}{\sqrt{ø_{nat}}} \qquad \text{Equation 6.4}$$

Where k_{acc} is the accelerated carbonation coefficient at 7.5% CO_2 concentration, and k_{nat} is the natural carbonation coefficient, $ø_{acc}$ and $ø_{nat}$ are CO_2 concentrations in accelerated and natural carbonation processes. The $ø_{nat}$ was taken as 0.04% (400 ppm) in India [296]. The carbonation depths after 14 and 28 days of CO_2 exposure and corresponding accelerated carbonation coefficients (k_{acc}) and natural carbonation coefficients (k_{nat}) are presented in Table 6.1.

Table 6.1 Carbonation depth and carbonation coefficients

Mix	Carbonation depth* 'x' (mm)		Carbonation coeficients	
	14 days carbonation	28 days carbonation	K_{acc} (mm/√day)	K_{nat} (mm/√year)
CC	6.3	10.5	1.92	2.69
MK10	5.9	9.5	1.75	2.45
NS1.5	5.1	8.6	1.58	2.20
NS3	4.3	7.6	1.38	1.93
NS4.5	5.4	8.3	1.54	2.14
MK10NS1.5	4.3	7.4	1.35	1.88
MK10NS3	3.9	6.8	1.25	1.74
MK10NS4.5	4.7	8.5	1.54	2.15

6.3.2 Water absorption

Figure 6.6 illustrates the water absorption (A) in different concrete mixes over time, measured by the mass increase of specimens when only one surface is exposed to water, as described in Chapter 5. The results show that the initial interaction between concrete and water is characterised by a notably high water absorption rate. However, with prolonged water exposure, this absorption rate gradually diminishes. Notably, after 6 days, the water absorption by the concrete samples virtually ceased, indicating a state of saturation within the internal pores of the concrete.

However, the specific properties of the samples play a significant role in how much water they absorb. The normal concrete exhibited relatively higher water absorption rates than the modified samples of MK and NS, with NS3 and MK10NS3 showing lower water absorption values over time among the binary and ternary mix, respectively. This suggests that the pozzolanic properties of MK and NS contributed to denser and more compact microstructures, leading to reduced capillary porosity.

At 7 days, MK10 concrete exhibited a 4% reduction in water absorption compared to CC. Similarly, NS1.5 and NS3 showed a 4.7% decrease in water absorption relative to the CC, while NS4.5 displayed a 4% reduction. Notably, the ternary mixtures yielded substantial reductions in water absorption, with MK10NS1.5 achieving a remarkable 13.5% reduction, MK10NS3 showing a significant 21% decrease, and MK10NS4.5 exhibiting a substantial 10% reduction in water absorption when compared to CC. This indicates that the synergistic effect between MK and NS led to the refinement of pores within the concrete and reduced water absorption. The water absorption results are thus consistent with the observed strength properties of the concrete mixes.

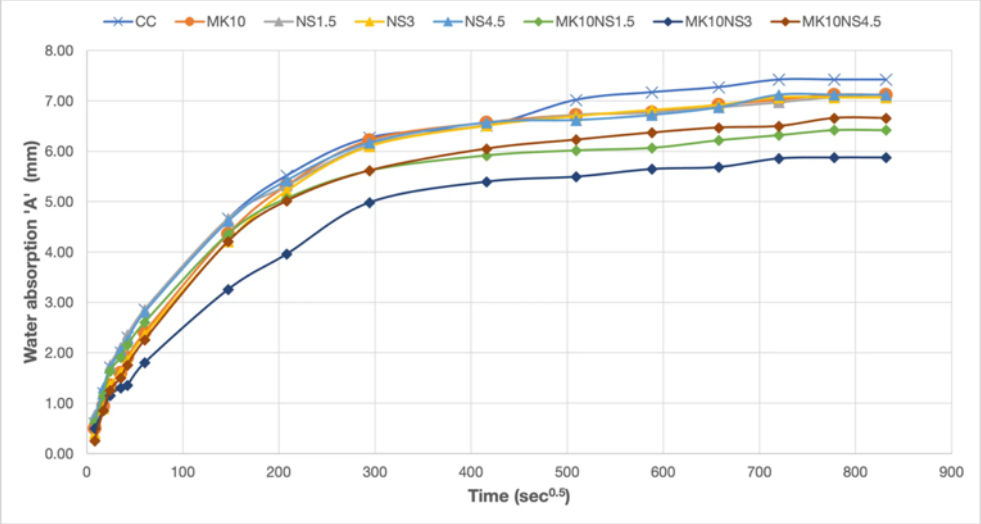

Figure 6.6 Rate of water absorption of the concrete mixes

Linear regression analysis was used to determine the initial and secondary rates of water absorption (Si and Ss). S_i is computed based on data spanning from 1 minute to 6 hours, while S_s is derived from data points ranging between 1 day and 7 days. Figure 6.7 to Figure 6.14 illustrate the regression plots showing the water absorption characteristics of the concrete mixes.

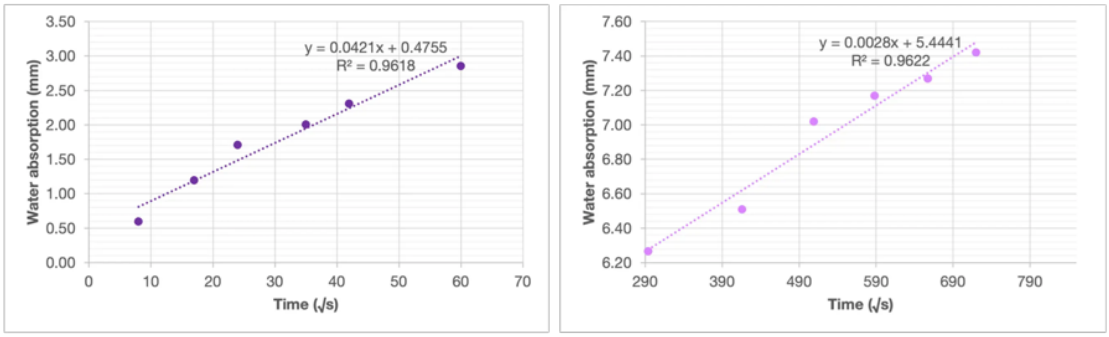

(a) (b)

Figure 6.7 Regression for initial (a) and secondary water absorption (b) of CC

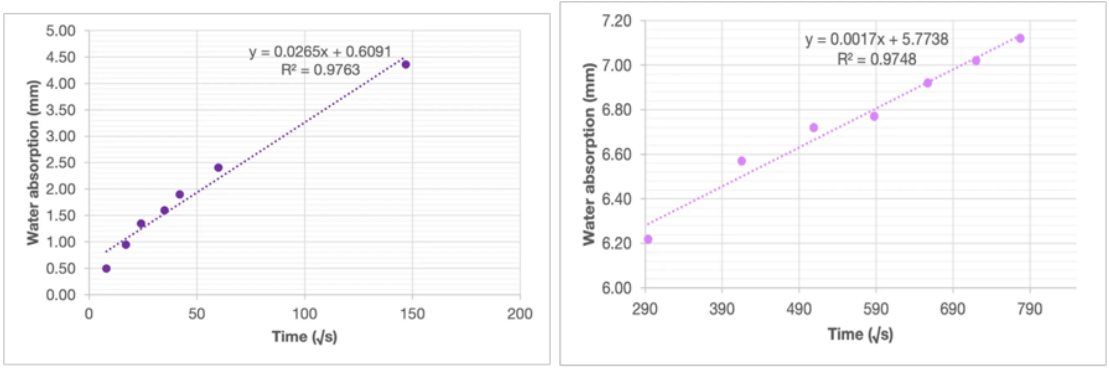

(a) (b)

Figure 6.8 Regression for initial (a) and secondary water absorption (b) of MK

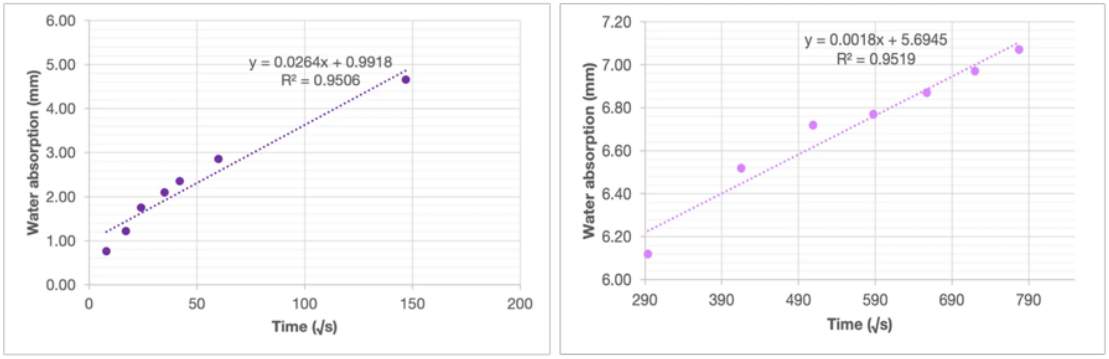

(a) (b)

Figure 6.9 Regression for initial (a) and secondary water absorption (b) of NS1.5

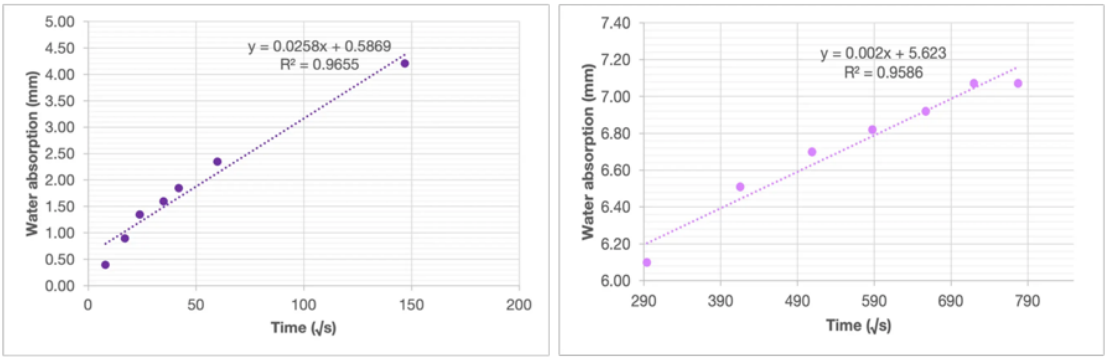

(a) (b)

Figure 6.10 Regression for initial (a) and secondary water absorption (b) of NS3

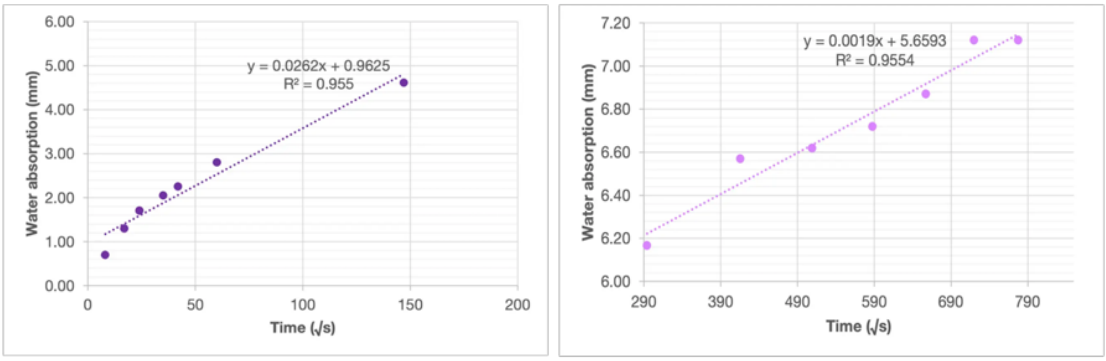

(a) (b)

Figure 6.11 Regression for initial (a) and secondary water absorption (b) of NS4.5

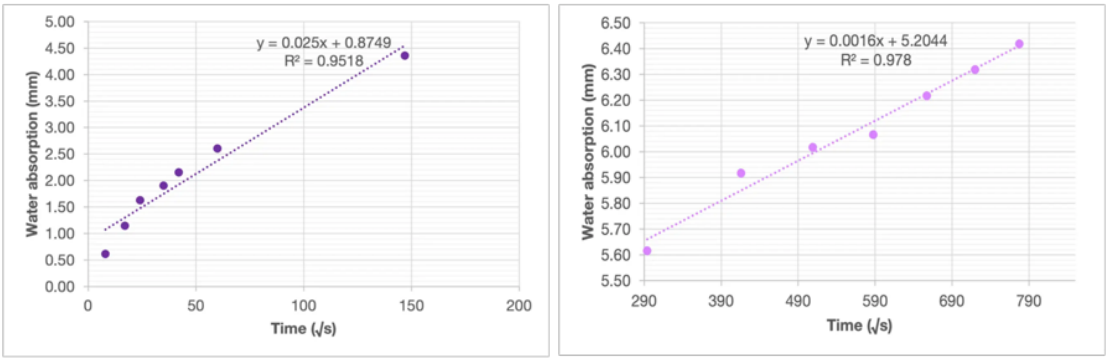

(a) (b)

Figure 6.12 Regression for initial (a) and secondary water absorption (b) of MK10NS1.5

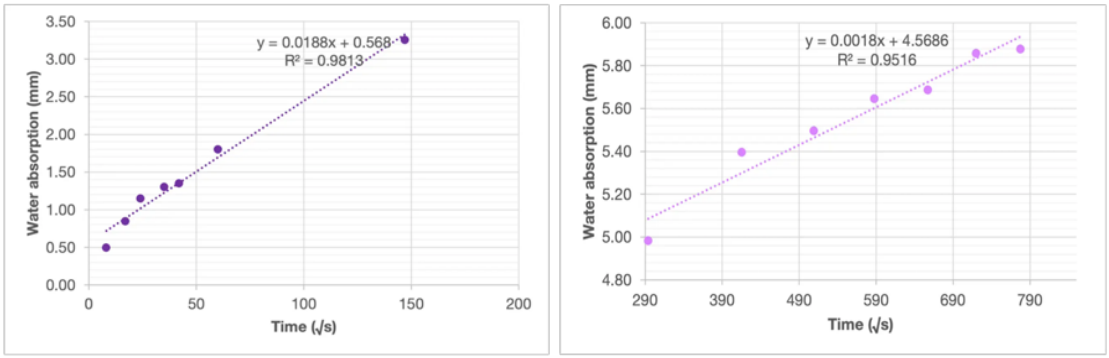

(a) (b)

Figure 6.13 Regression for initial (a) and secondary water absorption (b) of MK10NS3

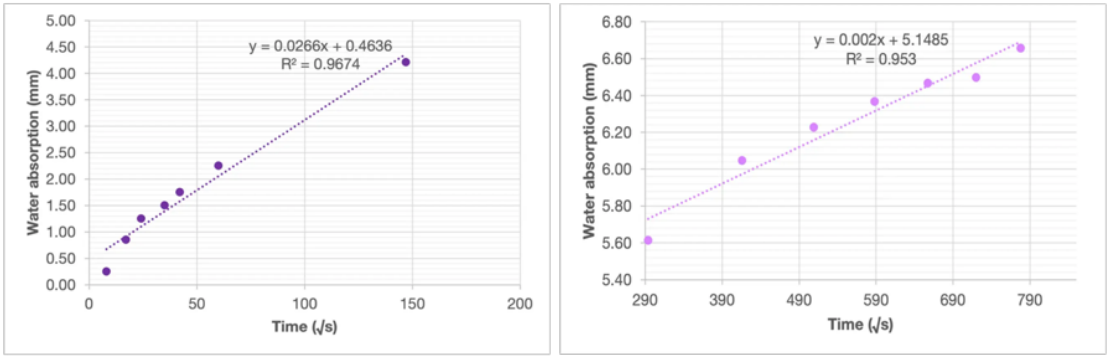

(a) (b)

Figure 6.14 Regression for initial (a) and secondary water absorption (b) of MK10NS4.5

Table 6.2 Rate of initial and secondary water absorption of different concrete mixes

Mix	Rate of initial absorption (mm/√s)	Rate of secondary absorption (mm/√s)
CC	4.21×10^{-2}	2.8×10^{-3}
MK10	2.65×10^{-2}	1.7×10^{-3}
NS1.5	2.64×10^{-2}	1.8×10^{-3}
NS3	2.58×10^{-2}	2×10^{-3}
NS4.5	2.62×10^{-2}	1.9×10^{-3}
MK10NS1.5	2.5×10^{-2}	1.6×10^{-3}
MK10NS3	1.88×10^{-2}	1.8×10^{-3}
MK10NS4.5	2.66×10^{-2}	2×10^{-3}

The initial and secondary water absorption rates in Table 6.2 for different concrete mixes provide valuable insights into the pore structure and water permeability of concrete samples.

A lower initial water absorption rate indicates a reduced concrete capillary porosity. MK10NS3 exhibited the lowest initial rates, implying a more refined and less porous microstructure. Similarly, a lower secondary water absorption rate indicates better durability and long-term resistance to water penetration. MK10NS1.5 has the lowest secondary rate, suggesting a significant pore structure refinement and reduced permeability enhancement. However, it's important to note that NS4.5 has a comparatively higher secondary rate, which might indicate that excessive NS did not contribute to refining the concrete microstructure.

6.3.3 Acid attack

The resistance of the concrete mix against the acid attack was measured in terms of mass loss of the concrete specimens after 28 days of their exposure to a 5% sulphuric acid solution. Figure 6.15 illustrates the percentage mass loss for the concrete mixes. The decrease in mass observed in the concrete specimens resulted from the dissolution of the bulk cement paste caused by the action of sulfuric acid, leading to partial leaching [297]. Normal concrete displayed a notably higher mass loss of 11.7%. However, the blended concrete mixes exhibited a promising trend of reduced mass loss, highlighting their enhanced resistance against aggressive acidic environments, attributed to the decreased permeability of the blended concrete mixes due to the pozzolanic activity.

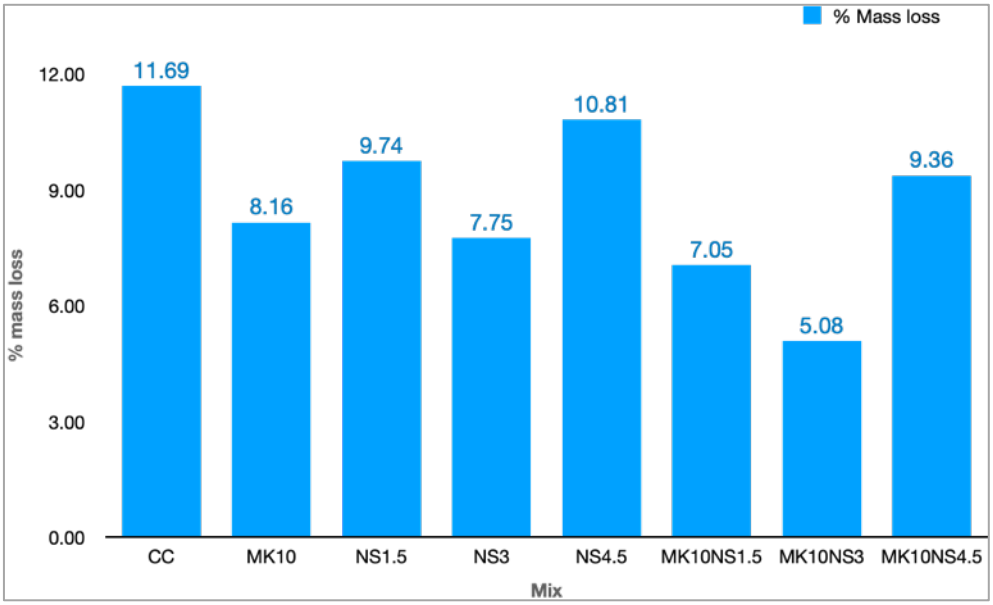

Figure 6.15 Concrete mass loss after 28-day sulfuric acid exposure

Furthermore, the variations in mass loss align with the outcomes observed in the water absorption tests. Specifically, when comparing binary mixes consisting solely of MK or NS to their ternary counterparts, the latter demonstrated superior resistance against sulfuric acid attack. The MK10NS3 concrete exhibited the lowest mass loss of just 5.08%, whereas MK10 and NS3 binary mixes recorded mass losses of 8.16% and 7.75%, respectively. When comparing the ternary MK10NS4.5 mix to the binary NS4.5 mix, the difference in weight loss was minimal, with values of 10.81% and 9.36%, respectively. This underscores the notion that higher dosages of NS did not result in a denser concrete microstructure, likely due to the agglomeration of NS particles.

The results thus emphasise the potential of MKNS blended concrete mixes, specifically in their ternary formulations, in enhancing concrete's resistance to acid-induced deterioration. The specimens of CC and MK10NS3 under acid attack are shown in Figure 6.16.

Figure 6.16 Concrete cubes after 28 days of sulfuric acid exposure

6.4 Microstructural analysis

6.4.1 X-ray diffraction (XRD) analysis

The obtained diffractograms illustrate XRD patterns of finely powdered cement pastes cured for 28 days, revealing the presence of portlandite, silicates, calcites, and ettringites. All samples consistently observed portlandite, highlighting its significant formation during cement hydration. When examining a typical XRD pattern, the horizontal scale, representing the diffraction angle, provides information about the crystal lattice spacing, while the vertical scale, denoting peak height, indicates the intensity of the diffracted ray. Notably, portlandite's (CH) intensity peak at a 2θ angle of 18° on the XRD scale was identified as a crucial performance indicator for cement paste samples. The XRD analysis further affirmed the positive impact of incorporating MK and NS together in concrete. Specifically, in the case of the CC sample, representing OPC without additives, the intensity peak reached 3900 counts (Figure 6.17a). In contrast, the MK10 blended cement paste exhibited a portlandite peak with an intensity count of 1984, indicating a 49% higher consumption of portlandite compared to the CC sample in the formation of CSH (Figure 6.17b). Likewise, the binary cement pastes incorporating NS at dosages of 1.5%, 3%, and

4.5% displayed portlandite peaks with intensity counts of 1950, 1492, and 1663, respectively (Figure 6.17c-e). These findings signify a greater consumption of portlandite (50%, 62%, and 57%, respectively) in these blended cement pastes (NS1.5, NS3, and NS4.5) compared to CC, emphasising their enhanced CSH formation potential.

The ternary blended pastes, MK10NS1.5, MK10NS3, and MK10NS4.5, exhibited distinct counts of 935, 484, and 962, respectively, as seen in diffractograms (Figure 6.17f-h), signifying a substantial increase in CH consumption compared to CC, with increments of 76%, 88%, and 75%, respectively. This observation underscores the synergistic impact of MK and NS in fostering elevated pozzolanic reactivity, resulting in the augmented formation of additional CSH gel.

XRD is less effective at creating distinct peaks for CSH phases because CSH is typically amorphous, lacking a well-defined crystal structure. XRD relies on the constructive interference of X-rays from regularly spaced atomic planes within a crystalline lattice. In the case of CSH, its structure is disordered, with irregularly distributed calcium, silicon, and oxygen atoms. This disorderly arrangement scatters X-rays randomly, resulting in broad, diffuse patterns instead of sharp peaks.

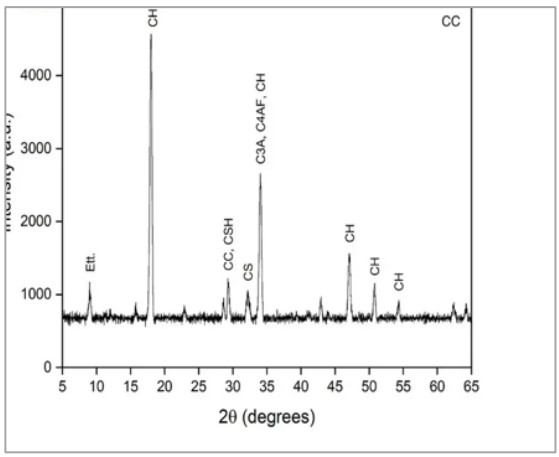

(a)

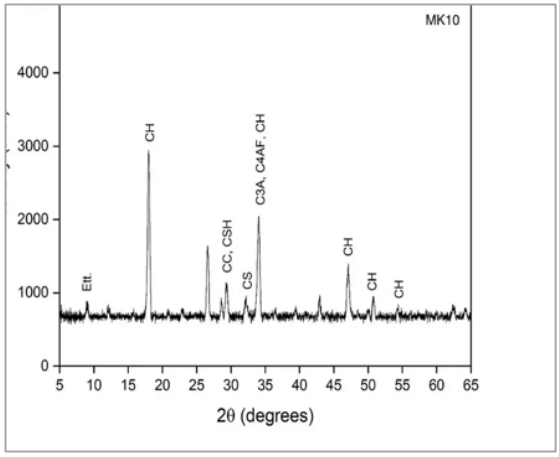

(b)

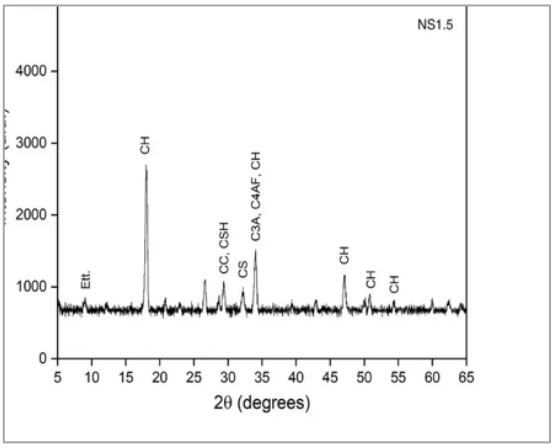

(c)

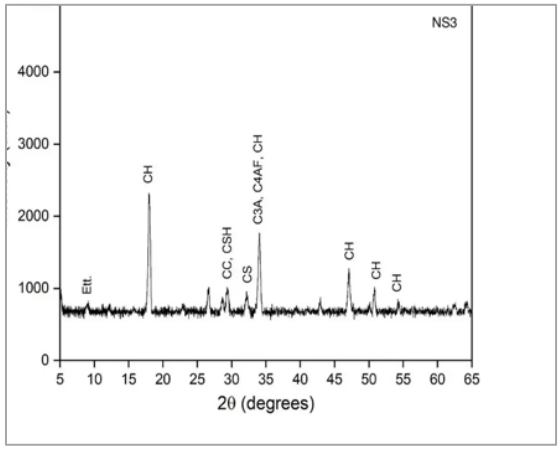

(d)

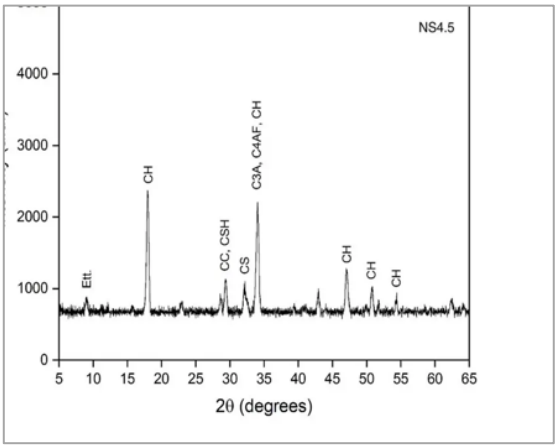

(e)

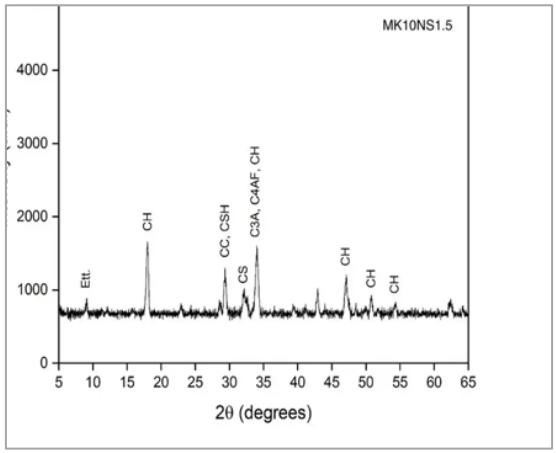

(f)

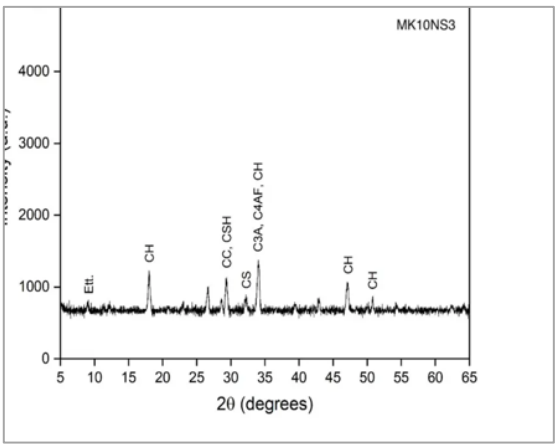

(g)

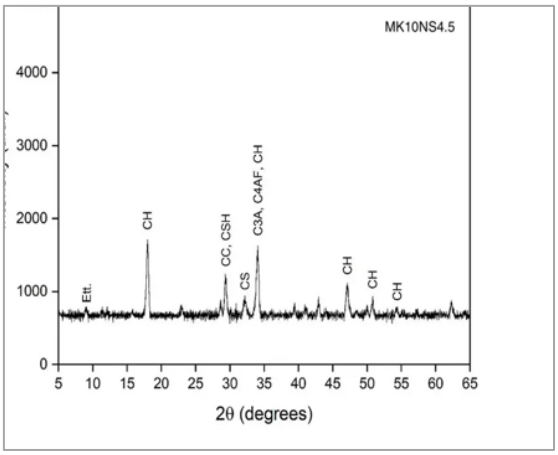

(h)

Figure 6.17 Diffractograms for different cement paste formulations after 28 days of curing

6.4.2 Thermogravimetric and differential scanning calorimetry (TGA/DSC) analyses

i ***TGA/DSC on cement paste cured for 28 days***

Table 6.3 displays the thermogravimetric analysis results for various blended cement pastes. Weight loss during the dehydration of hydration products occurs between 110-650°C and is proportional to the decrease in OPC content.

Table 6.3 Weight loss from TGA/DSC analyses

ID	%Weight loss*
CC	12.7
MK10	13.6
NS1.5	13.2
NS3	19
NS4.5	13.4
MK10NS1.5	14.3
MK10NS3	22.8
MK10NS4.5	13.2
*Weight loss in the range of 110-650°C	

The binary and ternary samples with 3% NS exhibited the highest weight loss, but further increasing NS dosage reduced weight loss. This increased weight loss may be due to the enhanced formation of CH and C3H in the pastes, possibly accelerated by NS particles, which aligned with the concrete compressive strength. The TGA/DSC curves are given in Figure 6.18.

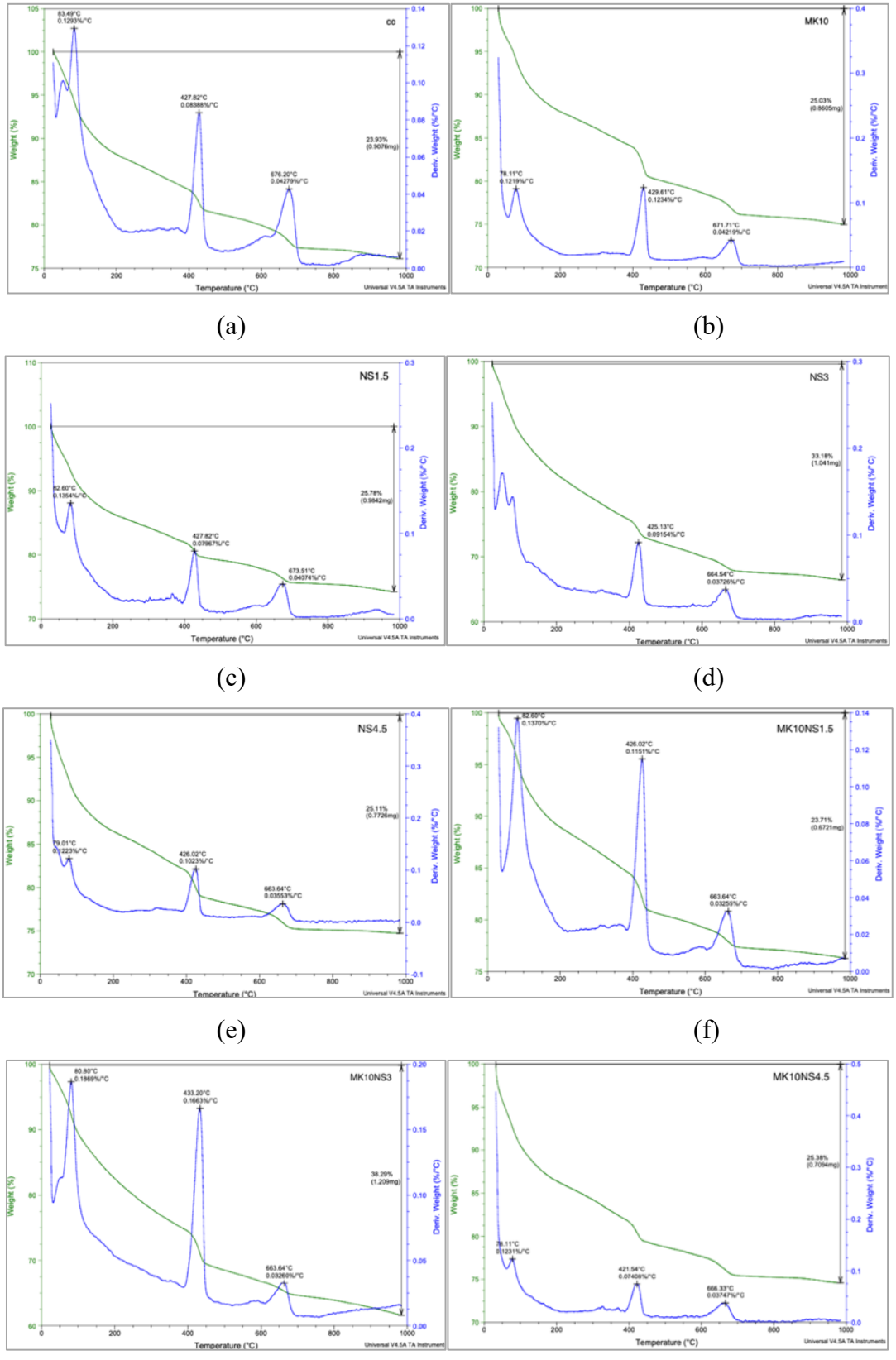

Figure 6.18 TGA/DSC curves for different cement paste formulations after 28 days of curing

ii ***TGA/DSC on extracts from the carbonated concrete cubes***

The TGA/DSC curves of the carbonated concrete are shown in Figure 6.19(a-h). Table 6.4 presents the weight loss and the corresponding $CaCO_3$ from the TGA analysis of the carbonated concrete. The weight loss occurring between 550°C and 950°C, attributed to $CaCO_3$ decomposition, correlates with the carbonation depths. The highest weight loss was observed in CC, while the lowest is observed in the MK10NS3 ternary mix, suggesting varying $CaCO_3$ content, with the normal concrete having the highest and MK10NS3 having the lowest $CaCO_3$ content.

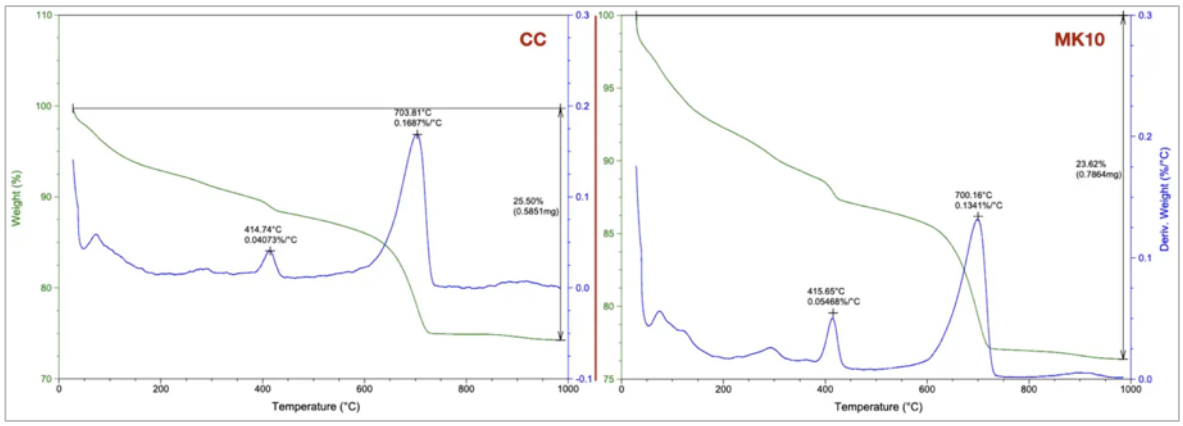

(a) (b)

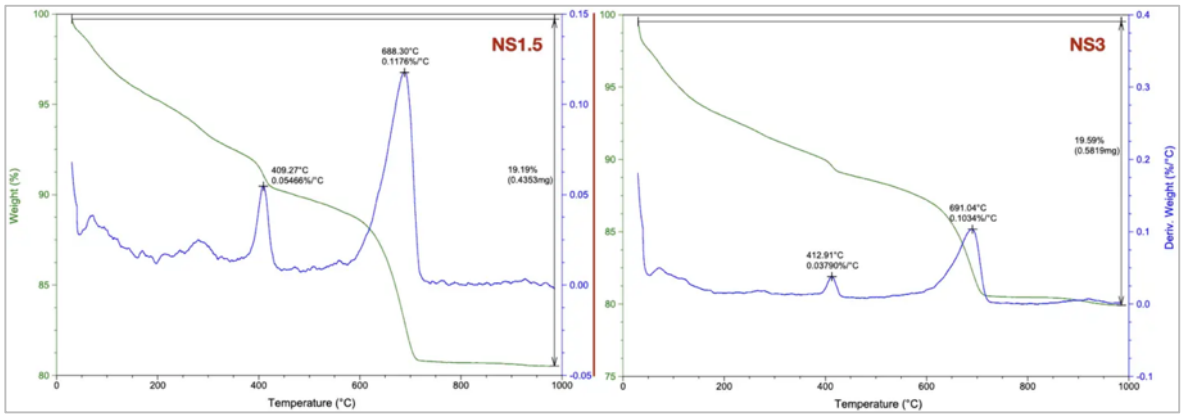

(c) (d)

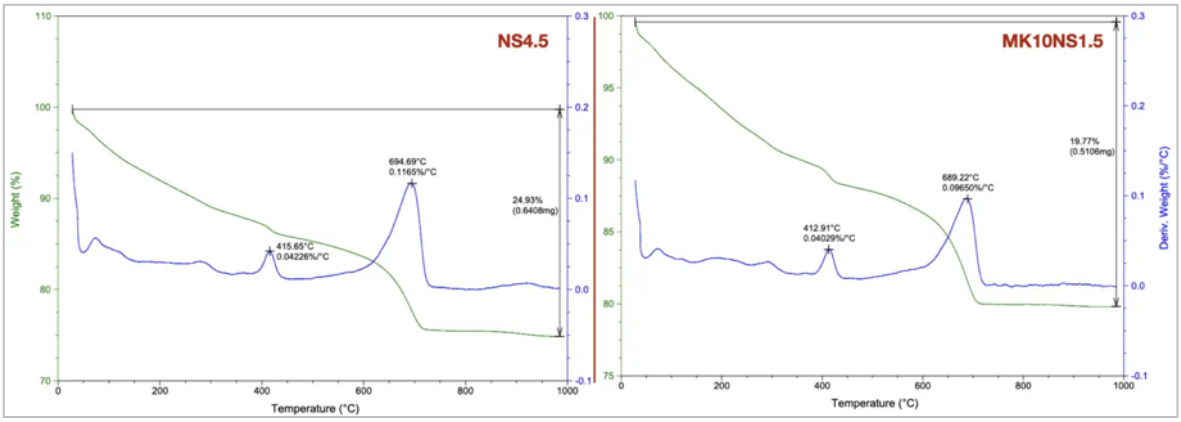

(e)

(f)

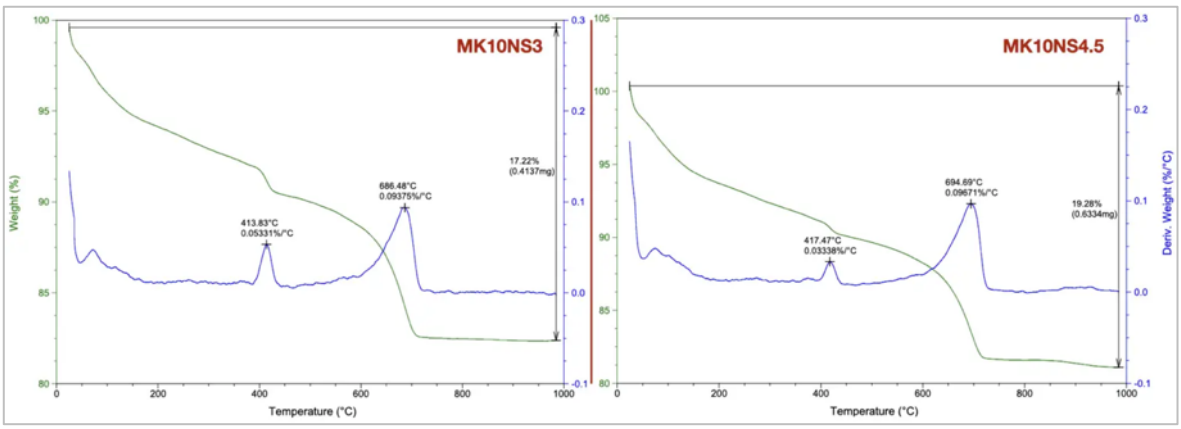

(g)

(h)

Figure 6.19 TGA/DSC curves for concrete samples carbonated for 28 days

Table 6.4 Quantified $CaCO_3$ Content Derived from TGA

Mix	% mass loss*	% amount of $CaCO_3$
CC	12.62	28.70
MK10	9.83	22.35
NS1.5	8.74	19.87
NS3	7.95	18.08
NS4.5	9.63	21.90
MK10NS1.5	7.41	16.86
MK10NS3	7.11	16.16
MK10NS4.5	7.93	18.03
Mass loss due to the decomposition of $CaCO_3$ occurs in between 550 and 950°C		

6.4.3 Scanning electron microscopic (SEM) analysis

The compressive strength of the concrete is influenced by its microstructure and can be explained with the help of SEM micrographs. SEM analysis was conducted on all blended cement pastes cured for 28 days. The micrograph (Figure 6.20) shows the presence of gel-like CSH and plate-like CH phases in CC samples. Ettringite (hydrous calcium aluminium sulfate mineral) was observed with micropores.

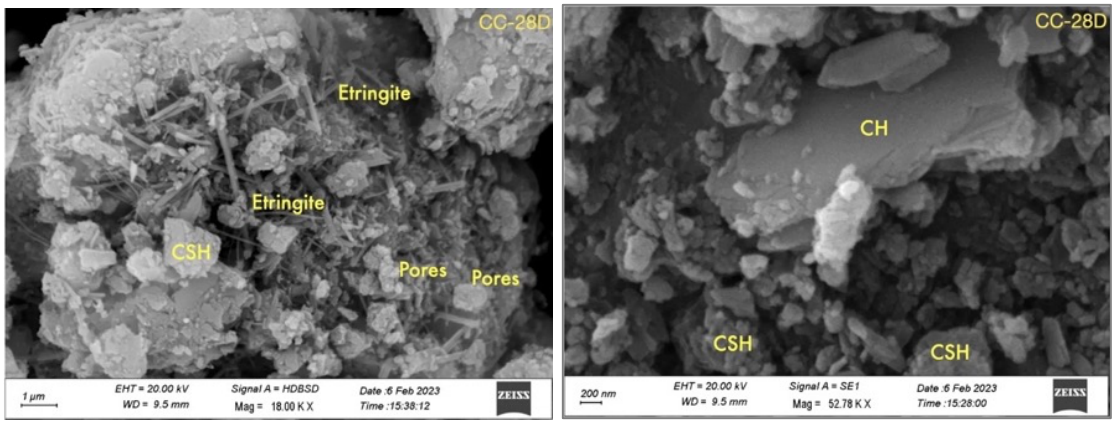

Figure 6.20 SEM images of CC paste-28 days

The SEM image (Figure 6.21) of MK10 shows a dense morphology of CSH gel as a dominant hydration product and calcium alumino-silicate hydrate (CASH) formed due to the high pozzolanic reactivity between MK and CH [298,299]. The CH phase and pores in the reference CC matrix highly disappeared in the MK10 matrix. The reaction of MK with CH forms the CSH and CASH. The reduction of ettringite was also noticed with the addition of MK, and the matrix became more uniform in its structure.

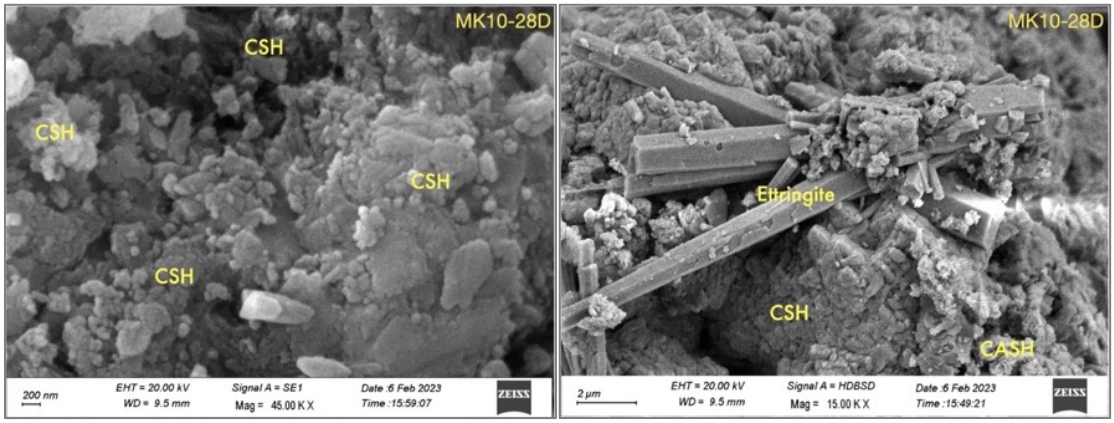

Figure 6.21 SEM images of MK10 blended paste-28 days

The SEM images of NS binary paste show that their microstructure was densified by incorporating silica nanoparticles. This can be attributed to the high pozzolanic activity of the NS particles with high surface area and their filling effect. The high pozzolanic activity causes the formation of extra CSH gel, and the filling effect results in the refinement of pores within the matrix and reduction in pore volume, thus causing a significant increase in the compressive strength of the concrete. The synergistic effect of NS particles and PCE (superplasticiser) also contributed to the mechanical strength.

SEM of NS1.5 (Figure 6.22) was observed with CSH as its main content. Needle-like ettringite formation was observed where the microstructure looks a little porous. The presence of calcite crystals was also observed in the matrix. Including PCE can influence the crystal nucleation, growth process, and formation of calcite crystals. The growing calcite crystals can also fill the voids, reduce the pore size, and make a more homogeneous and continuous matrix, causing the aggregates to be perfectly embedded within it [299].

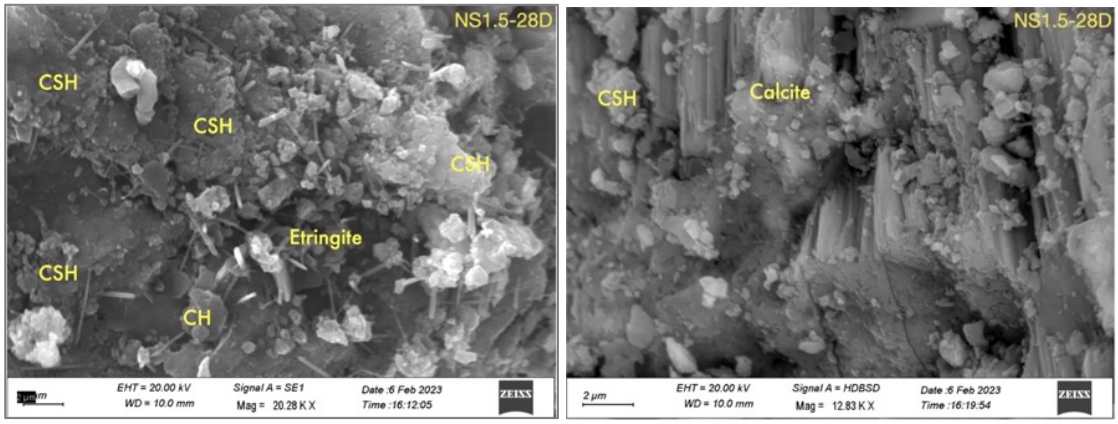

Figure 6.22 SEM images of NS1.5 blended paste-28 days

The combined effect of PCE and NS additives is particularly pronounced in NS3 mixtures, as evidenced by the SEM image (Figure 6.23) revealing distinct CSH structures resembling honeycombs or thin foils. When the precise dosage of these additives is introduced, their synergistic interplay leads to enhanced strength attributed to the deliberate reduction in pore size and ensuing decrease in porosity.

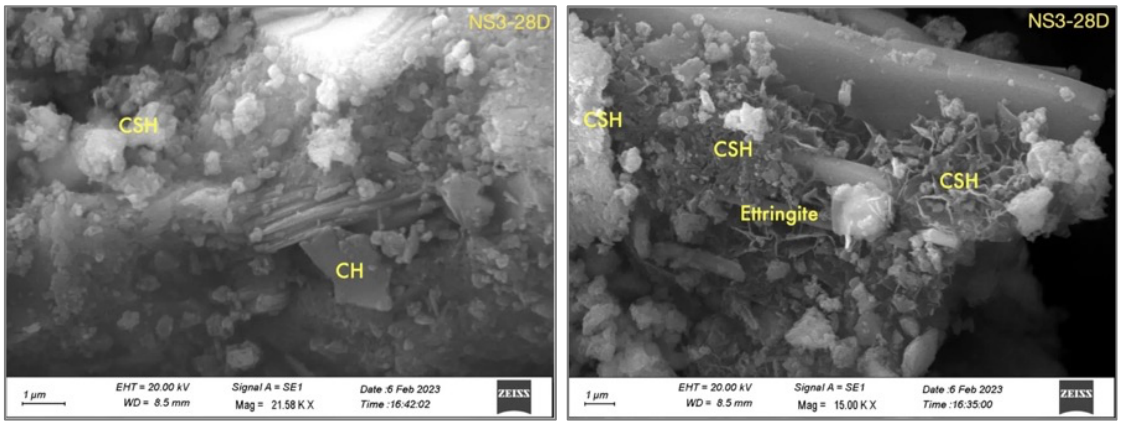

Figure 6.23 SEM images of NS3 blended paste-28 days

SEM image (Figure 6.24) of 4.5NS shows a scattered CSH gel in the matrix with CH. The presence of CH may be indicative of incomplete reactions in the concrete.

Additionally, more pores are observed in the mixture with 4.5% NS than the 3% counterpart, likely due to increased agglomeration, causing voids in the concrete.

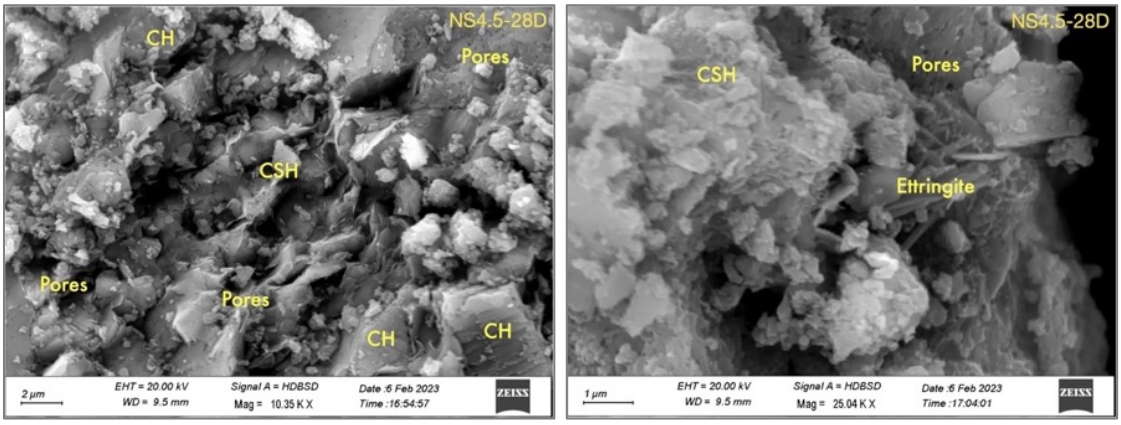

Figure 6.24 SEM images of NS4.5 blended paste-28 days

In the MK10NS1.5 mix, SEM (Figure 6.25) reveals the presence of CH hydration phases with a more predominant CSH gel. Pore sizes were more refined compared to the binary MK10 and NS1.5 mixes. This suggests that the combination of MK and NS enhanced the formation of the CSH gel, contributing to the strength. Smaller pore sizes indicate a more compact and less porous microstructure, which is generally favourable for concrete properties.

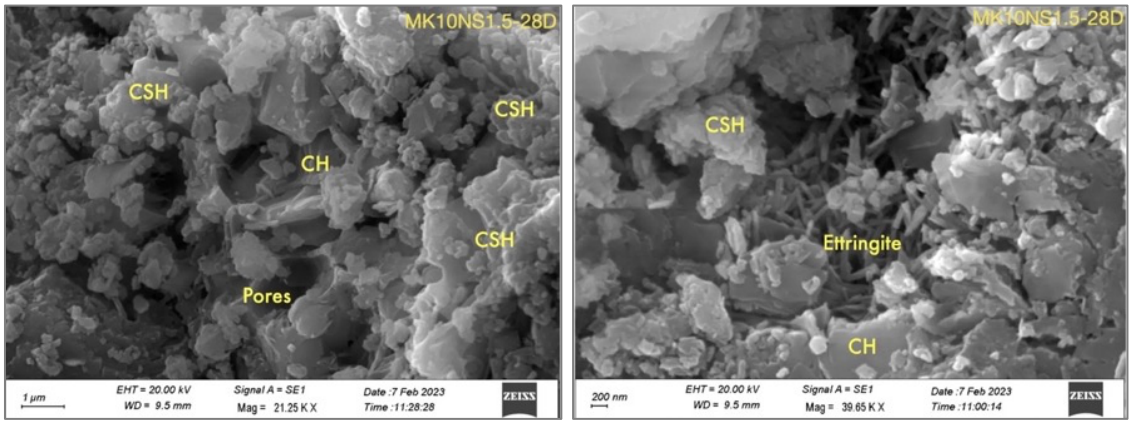

Figure 6.25 SEM images of MK10NS1.5 blended paste-28 days

In the MK10NS3 mix, SEM (Figure 6.26) shows a more densified microstructure compared to the MK10NS1.5 mix. A more uniform and compact matrix with CSH gel was observed, and pores were more refined due to the combined filler effect, MK hydration acceleration, and NS's pozzolanic activity. Increasing the NS content to 3% further improved the microstructure, with the denser matrix, refined pores, and NS's role in enhancing MK hydration and promoting pozzolanic reactions contributing to the improved microstructure. These SEM observations unequivocally support the significantly greater compressive strength of the MK10NS3 mix in comparison to the other mixtures.

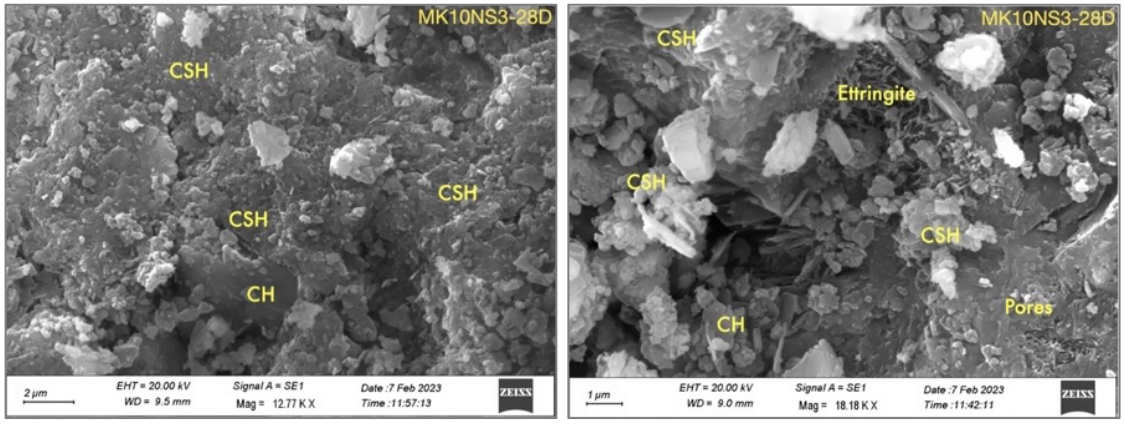

Figure 6.26 SEM images of MK10NS3 blended paste-28 days

Regarding the MK10NS4.5 mix, SEM (Figure 6.27) reveals a favourable morphological structure compared to its binary counterparts. However, there is a relatively higher presence of CH, which may be attributed to incomplete reactions in the concrete. Although adding 4.5% NS further enhanced the microstructure, the relatively high CH presence suggests possible agglomeration of NS particles, adversely impacting the pozzolanic reaction with CH.

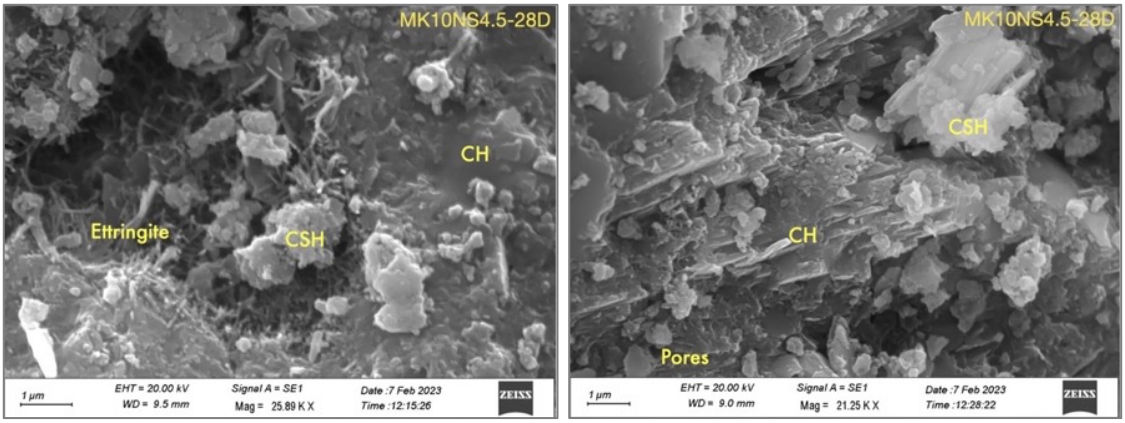

Figure 6.27 SEM images of MK10NS4.5 blended paste-28 days

From the above morphological analysis, it can be concluded that the ternary blend of cementitious pastes containing MK and NS leads to significant improvements in the microstructure compared to their binary counterparts. The predominant presence of CSH gel, refined pore structures, and a denser matrix indicate enhanced strength and durability.

6.4.4 Porosity by N_2 adsorption test (BET/BJH analysis)

Table 6.5 presents the results of the N_2 absorption test for the BET surface area, percentage porosity, and average pore diameter of cement paste powders from various mixes. The findings unequivocally show that including MK and NS led to a reduction in pore volume. The percentage porosity of the ternary mixtures, such as MK10NS1.5 and MK10NS3, was notably lower than their binary counterparts and normal mix, though the average pore diameter was increased. The higher surface area observed served as an indicator of increased voids.

These results from the N_2 adsorption test align with the outcomes of mechanical and durability tests, providing additional support to the notion that incorporating MK and NS positively influences the pore characteristics of the cement paste.

Table 6.5 Summary of BET/BJH analysis

Mix	BET surface area (m^2/g)	% Porosity (BJH)	BJH adsorption avg. pore dia. (nm)
CC	63.52	12.61	5.78
MK10	46.48	11.51	7.18
NS1.5	34.4	11.31	9.99
NS3	22.12	10.10	13.36
MK10NS1.5	29.33	8.99	9.01
MK10NS3	27.08	8.71	9.27

6.5 Thermal stability of concrete

6.5.1 Residual compressive strength

The residual compressive strength resulting from the unstressed residual test of concrete mixes at elevated temperatures is presented in Table 6.6

Table 6.6 Residual compressive strength of concrete mixes at different temperatures

Temp (°C) ▶ / Mix ▼	Residual compressive strength (MPa)					
	27±2°C	200°C	350°C	500°C	650°C	800°C
CC	59.1	61.6	62.1	63.4	38.0	20.6
MK10	64.6	70.2	72.3	60.6	39.5	22.7
NS1.5	66.1	67.6	76.6	60.9	38.1	26.1
NS3	71.1	73.8	73.6	64.6	40.3	20.2
NS4.5	64.8	66.9	67.2	59.4	39.3	16.7
MK10NS1.5	69.1	78.7	68.6	63.2	39.6	23.7
MK10NS3	75.9	81.1	74.4	67.9	38.9	18.0
MK10NS4.5	65.9	67.8	68.1	59.9	34.9	17.0
Residual strength is the strength that remains in concrete after heating						

Figure 6.28 illustrates the temperature-dependent variations in residual compressive strength for CC, binary and ternary concretes with MK and NS. Figure 6.29 illustrates the percentage change in residual strength of the concrete mixes resulting from heat exposure relative to their strength at room temperature.

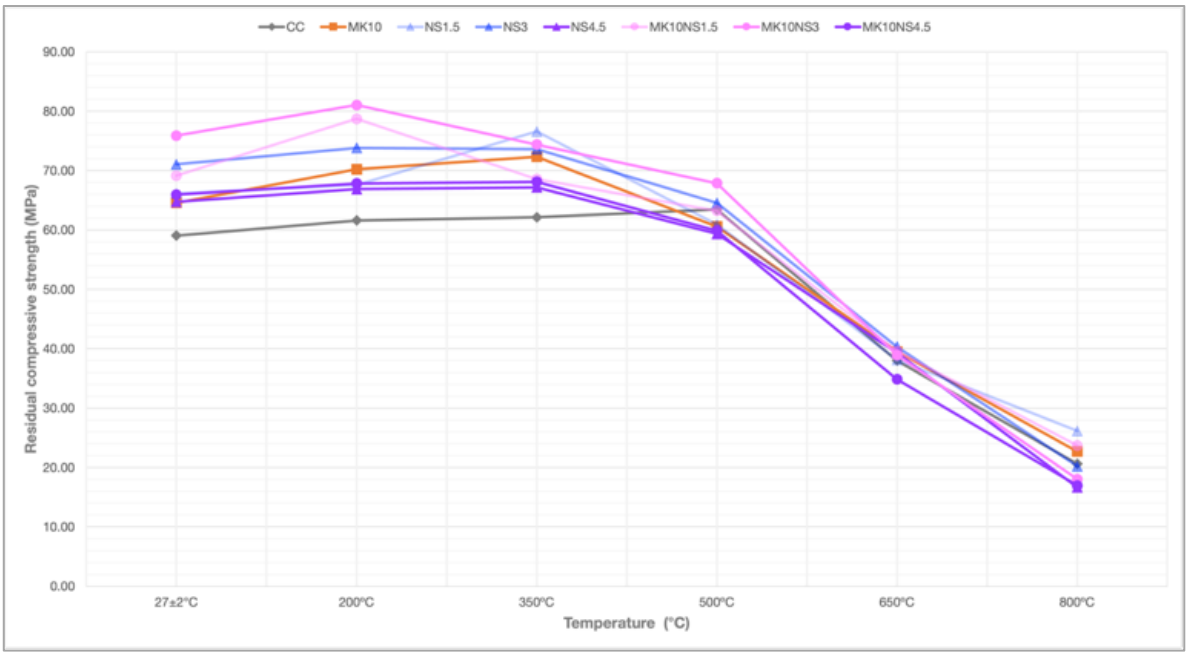

Figure 6.28 Residual compressive strength vs. temperature

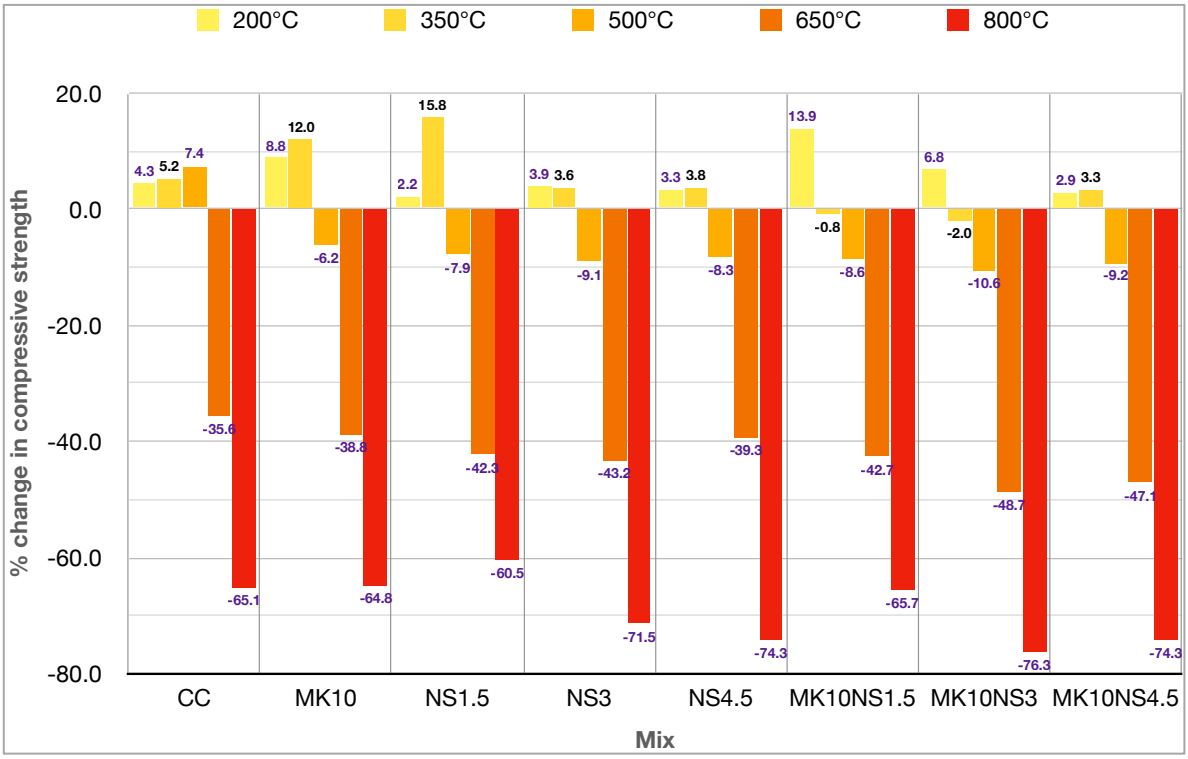

Figure 6.29 Percentage change in compressive strength at different temperatures

At an ambient temperature of 27±2°C, the 90-day compressive strength of CC was 59.1 MPa. Upon exposure to elevated temperatures up to 500°C, the compressive strength increased in CC. Heikal [300] reported a similar trend of increasing strength when the OPC concrete was subjected up to 500°C. At 200°C, a modest increase was observed, reaching the strength of 61.6 MPa. The strength exhibited a gradual ascent, reaching 62.1 MPa at 350°C. Notably, at 500°C, a discernible increase of 7.4% from its 90-day strength resulted in an elevated strength level of 63.4 MPa.

This enhancement is attributed to the additional hydration of unhydrated cement grains induced by steam under conditions akin to internal autoclaving in the cement paste [301]. A pronounced decline in compressive strength was observed as the temperature continued to rise. At 650°C, the compressive strength rapidly diminished to 38 MPa, indicating a substantial reduction of 36%. The escalation of temperature to 800°C induced a significant decrement in compressive strength to 20.6 MPa, indicating a considerable reduction of approximately 65%. The decline in compressive strength could be attributed to the dehydration of CH around 500 °C, resulting in the formation of CaO and H_2O. Strength deterioration beyond 650°C primarily arises from the dissociation of $CaCO_3$ and the subsequent release of CO_2 [301].

Incorporating 10% MK resulted in a notable increase in the compressive strength of concrete when exposed to elevated temperatures. Specifically, there was a substantial improvement of about 9% and 12% at 200°C and 350°C, respectively, compared to the baseline strength of 64.6 MPa at ambient temperature. However, the compressive strength of the MK10 concrete exhibited a diminishing trend as the temperature continued to rise beyond 350°C. Notably, a 6% reduction was observed at 500°C, followed by more

pronounced decreases of 39% and 65% at 650°C and 800°C, respectively. This led to final strengths of 39.5 MPa and 22.7 MPa at these elevated temperatures.

The introduction of NS positively influenced the compressive strength of its binary compositions, particularly at temperatures up to 350°C. At 200°C, NS1.5, NS3, and NS4.5 mixes exhibited increases of approximately 2.2%, 4%, and 3.3%, respectively. At 350°C, further improvements were observed, with increments of 16%, 3.6%, and 3.7%, resulting in compressive strengths of 76.6 MPa, 73.6 MPa, and 67.2 MPa for NS1.5, NS3, and NS4.5 mixes, respectively. While there was a slight decrease in the percentage increase in compressive strength at 350°C in the NS3 mix, it still surpassed its initial compressive strength at room temperature. The compressive strength of all NS binary concrete compositions experienced a continuous decline beyond 350°C. At 500°C, reductions were approximately 7.8%, 9%, and 8.3% for NS1.5, NS3, and NS4.5%, resulting in strengths of 60.9, 64.6, and 59.4 MPa, respectively. A substantial reduction of 42%, 43%, and 39% occurred at 650°C, and within the 650-800°C range, a severe loss of strength was observed, leading to reductions of 60.5%, 71.5%, and 74.3% in NS1.5, NS3, and NS4.5% concrete cubes, yielding strengths of 26.1, 20.2, and 16.7 MPa, respectively.

The compressive strength of ternary concrete mixes exhibited an upward trend with increasing temperatures up to 200°C. Notably, MK10NS1.5, MK10NS3, and MK10NS4.5 registered percentage increases of 13.9%, 6.8%, and 2.9%, respectively. This translated to final strengths of 78.7 MPa, 81.1 MPa, and 67.8 MPa. Upon reaching 350°C, a slight decline in compressive strength was observed for MK10NS1.5 and MK10NS3, approximately 1% and 2% lower than their initial strengths, resulting in

strengths of 68.6 MPa and 74.4 MPa, respectively. In contrast, MK10NS4.5 displayed a marginal increase of 3%, reaching a strength of 68.1 MPa. Between 500°C and 800°C, a significant reduction in compressive strength was evident across all ternary mixes. Specifically, MK10NS1.5 experienced reductions of 8.6%, 42.7%, and 65.7%, while MK10NS3 exhibited the highest strength loss at 10.6%, 48.7%, and 76.3% at 500°C, 650°C, and 800°C, respectively. At 800°C, MK10NS1.5 and MK10NS3 achieved strengths of 23.7 MPa and 18 MPa, respectively. Similarly, MK10NS4.5 underwent a strength reduction of 9.2%, 47.1%, and 74.3% at 500°C, 650°C, and 800°C, ultimately reaching a value of 17 MPa at 800°C.

In MK blended cement concrete, the increase in compressive strength can be ascribed to the temperature-induced hydration of the unhydrated MK particles and their filler effect [301,302]. The decline in compressive strength beyond 350°C could be ascribed to the dehydration of CH at 400°C; upon reaching 650°C, the concrete experienced degradation, resulting in a substantial reduction in compressive strength. This phenomenon can be linked to the diminished binding efficiency caused by the dehydration of the CSH gel [303]. In NS blended concrete, the strength increase with a temperature rise to 350°C can be ascribed to the continued hydration of unreacted cement particles with NS particles, improving the concrete microstructure [304]. The notable residual compressive strength observed in the MKNS ternary mix can be attributed to its denser microstructure due to the synergistic effect between MK and NS.

Vapour emanates from water adsorbed in capillary pores and bound water within the cement paste at elevated temperatures. This initiates an autoclaving reaction within the cement pastes, enhancing the pozzolanic reaction between MK and NS particles with CH.

The outcome is the formation of additional CSH characterised by a low Ca/Si ratio, contributing to heightened strength properties [305,306]. The reduction in compressive strength observed above 350°C is ascribed to the degradation of cementitious materials and the expansion of the water layer within the cement paste. Additionally, the heightened temperature contributes to an augmentation in the porosity of the cement paste, resulting from pore structure coarsening, thereby enhancing the permeability of the concrete [305]. Also, enhanced strength diminished at elevated temperatures of 650°C and 800°C due to the development of high vapour pressure within the compact concrete structure. This pressure induces the formation of microcracks, potentially compromising the concrete's overall strength [307-309]. The pozzolanic type and dosage of pozzolanic materials can significantly influence the residual strength [301].

The deterioration of concrete's compressive strength was also closely associated with the breakdown of aggregates. When subjected to thermal stress surpassing their yield strength, aggregates undergo the development of microcracks. This phenomenon, known as thermal rupture, ensues from the uneven expansion of mineral particles due to heat stress, leading to aggregates breaking. The initiation of microcracks occurs at 200°C, and as the temperature rises to 300°C, these microcracks progressively interconnect, forming a network of cracks. Ultimately, this interconnected network results in the cracking of aggregates at 500°C [310].

6.5.2 Mass loss

The mass loss of the concrete compositions was analysed by comparing their masses before and after heating. The mass loss of the sample that underwent explosion was also considered. As the temperature increased, there was a corresponding rise in mass loss.

Furthermore, a concurrent increase in mass loss with an increase in cement replacement was also observed. The mass loss of the samples is illustrated in Figure 6.30. The results suggest a significant rise in the rate of mass loss between temperatures of 27±2°C and 350°C compared to the mass loss observed between 350°C and 800°C.

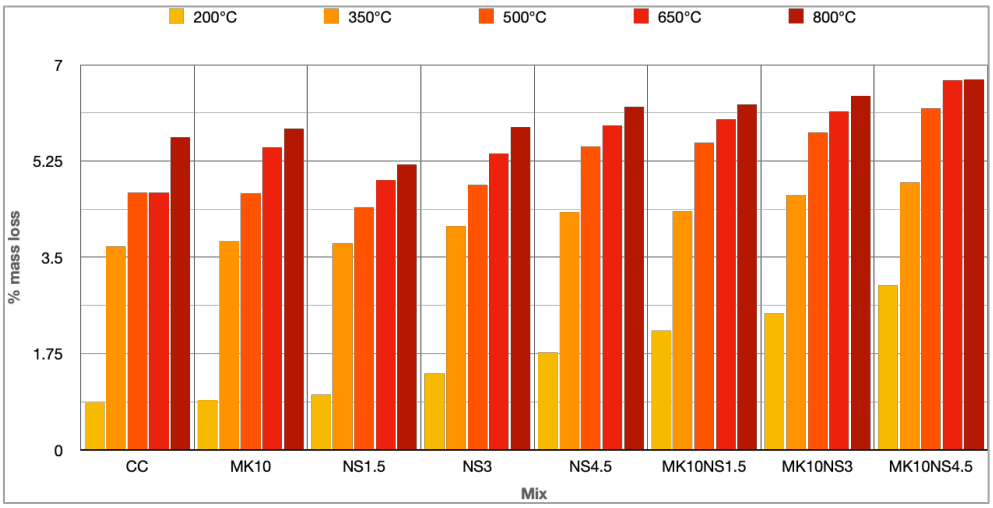

Figure 6.30 Percentage mass loss of the concrete samples at different temperatures

The general trend of mass loss at elevated temperatures, up to 200°C, can be ascribed primarily to the expulsion of evaporated water and the liberation of free water residing in the capillary pores. As the temperature rises to 400 °C, this mass reduction was likely a consequence of water elimination within chemical bonds, indicative of the decomposition of carboaluminate hydrates. Notably, by 400 °C, the entire capillary water was depleted. The inevitability of mass loss becomes pronounced beyond 600 °C, where the breakdown of most of the bonds within the CSH gel was anticipated [311]. This mass loss was due to the evaporation of chemically combined water, which was released during the decomposition of the hydration product at 500°C. The evaporation of this water was very difficult, and therefore, the rate of mass loss was comparatively low, between 600-800°C

[302]. The decomposition or decarbonisation of CH at the temperature range of 400-500°C also caused mass loss in the concrete [311].

Additionally, the transformation of low quartz (alpha quartz) to high quartz (beta quartz) at 573°C induces the expansion of quartz aggregates (sand). This transformative process induces cracking at the interface between the paste and aggregates, leading to subsequent mass loss in the concrete [304].

6.5.3 Thermal resistance

The thermal resistance of the concrete samples was evaluated by comparing the areas under the curve of the relative strength of the respective concrete mixes as proposed by Abdelmelek and Lubloy [312]. The relative residual compressive strength was determined as the ratio of concrete strength at elevated and room temperatures and represented by the line graph, as shown in Figure 6.31.

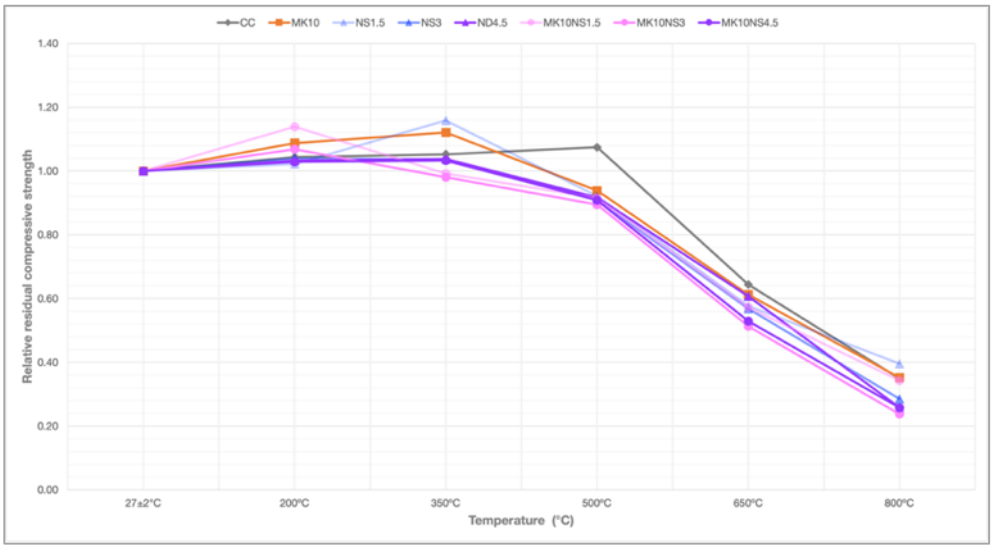

Figure 6.31. Relative residual compressive strength vs. temperature

The area under the residual relative curve of each concrete mix represented as the thermal resistance of the respective sample is shown in Figure 6.32. The curve areas provide insight into the performance of each concrete under elevated temperatures.

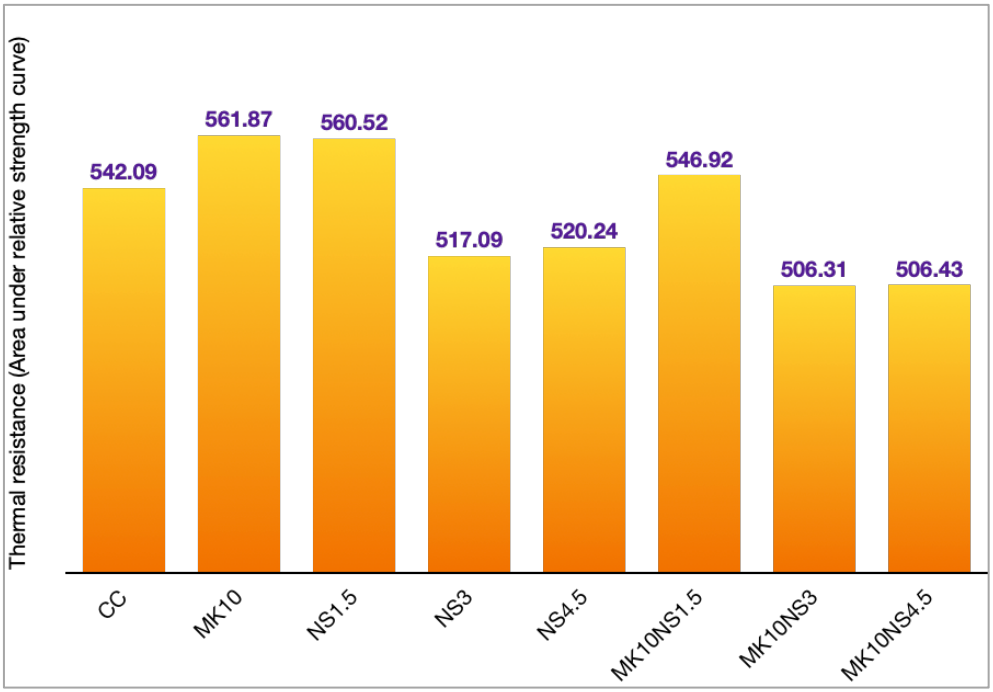

Figure 6.32 Area under residual compressive strength curve of concrete

The MK10 specimen demonstrated the highest area under the curve of residual compressive strength, signifying superior thermal resistance within the sample set. The NS1.5 sample closely followed MK10, exhibiting comparable resistance against heat. Notably, the MK10NS1.5, with a value of 546.92 in the ternary mix, displayed resistance surpassing that of ordinary concrete. These findings imply the effectiveness of MK10, NS1.5, and MK10NS1.5 in preserving strength under elevated temperatures compared to normal concrete.

6.5.4 Surface cracking and spalling

Figure 6.33 to Figure 6.38 show the cracks on the concrete surface after exposure to high temperatures. All the concrete samples heated over 350°C underwent discolouration, turning into light grey, yellow, or pink, as seen in the figure. Concrete undergoes chemical and physical changes at elevated temperatures according to their exposed temperature level. No visible surface cracks were noted on the concrete specimens subjected to temperatures up to 200°C, consistent with the findings by [313]. However, several networks of slender cracks were detected in most concrete samples exposed to 350°C. Both normal and blended cement concrete of NS and MK exhibited identical surface crack formation and overall surface appearance, except for colour variations. After exposure to 500°C, surface observations revealed minor scratches and relatively visible cracks on the concrete specimens due to their direct exposure to the high temperature. In Figure 6.33 and Figure 6.34 the cracks are highlighted in the boxes.

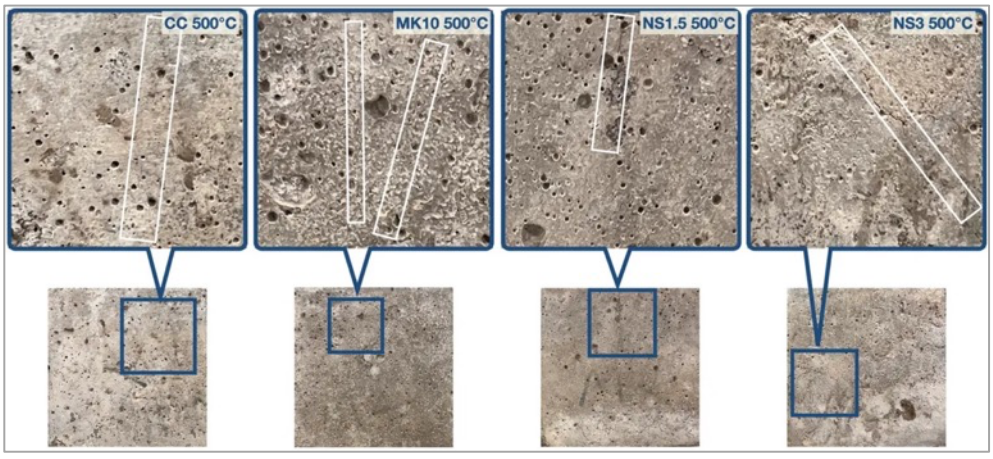

Figure 6.33 Concrete cube surface at 500°C-CC, MK10, NS1.5 and NS3

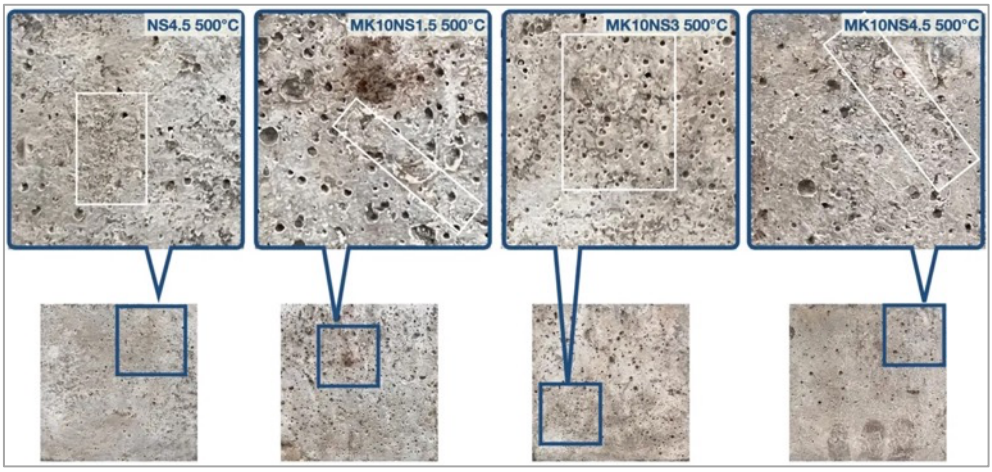

Figure 6.34 Concrete cube surface at 500°C-NS4.5, MK10NS1.5, MK10NS3 and MK10NS4.5

As the temperature rose to 800°C, the size of the cracks was noted to expand, with both width and length showing an increase. The development and spreading of these cracks were contingent upon internal vapour pressure, wherein the increase of pore pressure [314] due to the temperature rise led to the formation of broader and more extensive cracks.

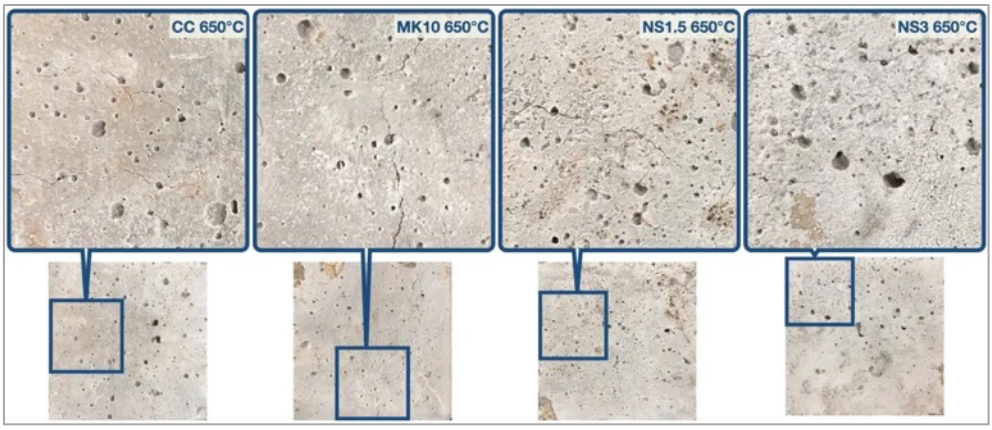

Figure 6.35 Concrete cube surface at 650°C-CC, MK10, NS1.5 and NS3

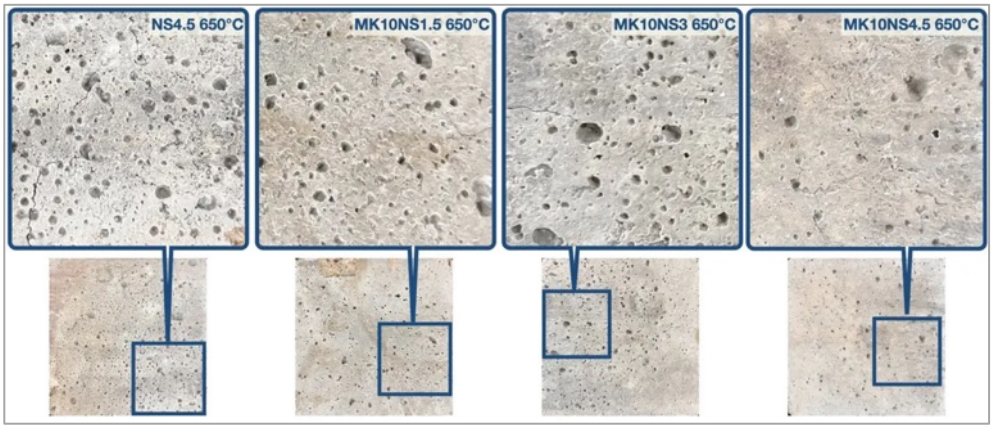

Figure 6.36 Concrete cube surface at 650°C-NS4.5, MK10NS1.5, MK10NS3 and MK10NS4.5

The ternary mix MK10NS4.5 displayed decreased surface cracking at 650 and 800°C, with explosive spalling observed in one specimen at 650°C (Figure 6.39). This affirms the accumulation of internal vapour pressure within the dense cement paste, limiting moisture release and leading to heightened pressure and eventual spalling.

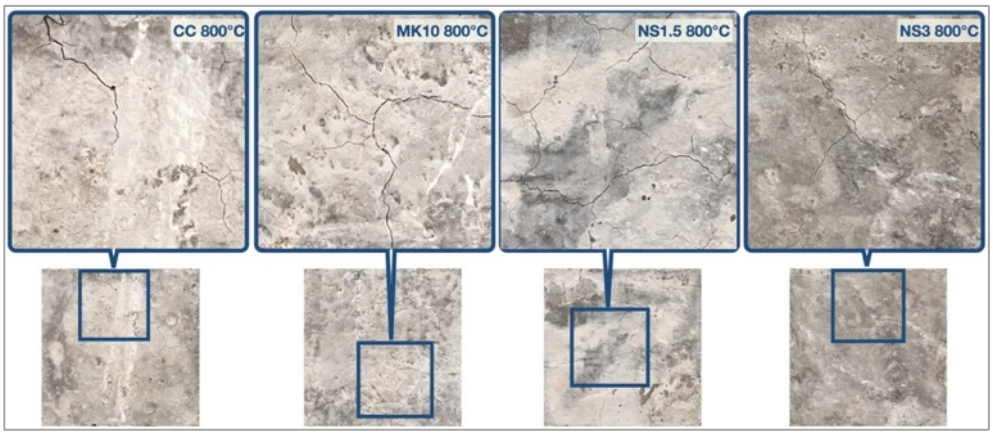

Figure 6.37 Concrete cube surface at 800°C-CC, MK10, NS1.5 and NS3

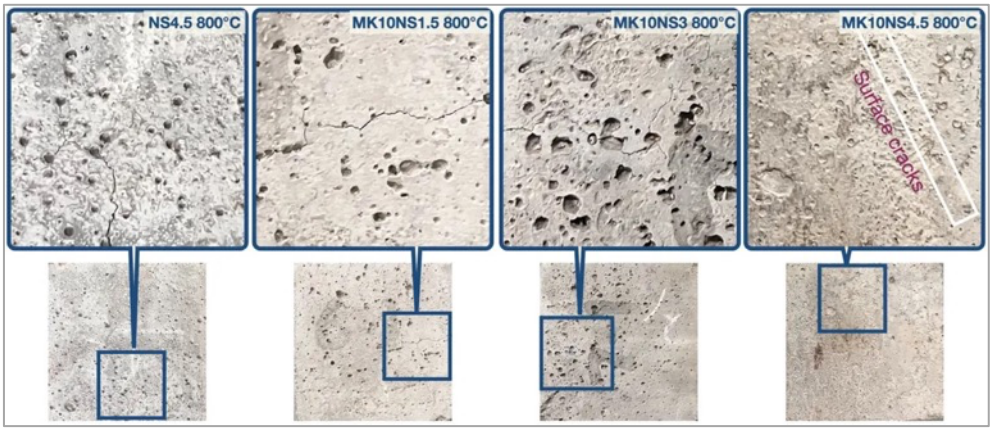

Figure 6.38 Concrete cube surface at 800°C-NS4.5, MK10NS1.5, MK10NS3 and MK10NS4.5

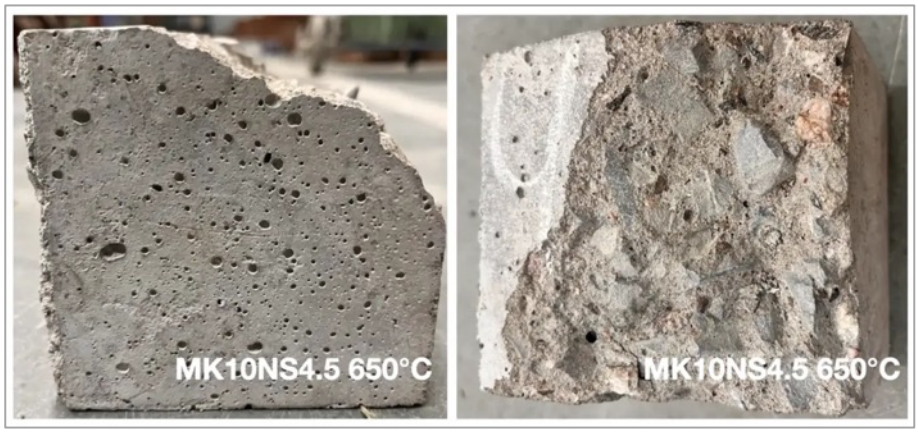

Figure 6.39 Spalled cube of MK10NS4.5 at 650°C

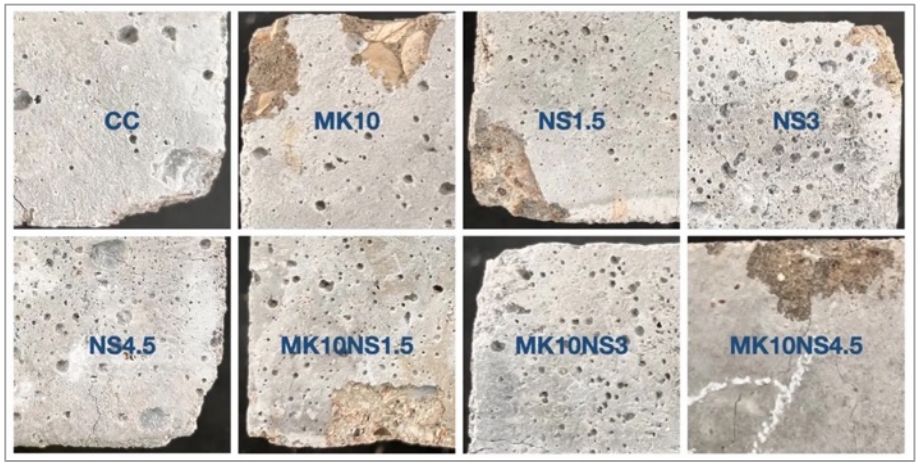

Figure 6.40 Ablation of the concrete cube surface layer at 800°C

At a temperature of 800°C, all concrete samples exhibited ablation of their surface layer due to the high thermal compressive stress parallel to the heated surface [268] as shown in Figure 6.40.

6.6 Microstructural analyses on concretes exposed to elevated temperatures

6.6.1 X-ray diffraction (XRD) analysis

The diffractograms of different concrete samples after exposure to different temperatures, enumerating the analysed peaks at various temperatures, are shown in Figure 6.41a-h. Except for the reference sample, CC, the diffractograms of all samples exhibited the ettringite peak 'E,' typically dehydrated within the temperature range of 110°C to 150°C [315]. The reference sample displayed a notably high portlandite peak, 'P,' whereas the blended cement concrete demonstrated a lower portlandite peak, with ternary MKNS mixes exhibiting the lowest peak. This can be attributed to the pozzolanic reaction of MK and NS, leading to CH consumption.

The decline in the portlandite peak with an increase in temperature signifies its decomposition, occurring at 400-500°C. Notably, certain samples (MK10, NS1.5, NS3, NS4.5 and MK10NS1.5) exhibited an increase in the portlandite peak within the temperature range of 350-500°C, attributed to late hydration resulting from the disintegration of CSH [315]. As temperature rises, MK10 and NS1.5 samples showed slightly higher portlandite peaks than NS3, NS4.5, and MK10NS1.5. The XRD peaks, therefore, are in line with residual compressive strength.

The loss of water by CH from 400°C to 500°C led to its decomposition into calcium oxide (CaO), and if CO_2 is available above 400°C, it can form $CaCO_3$ [316]. This explains the observed increase in the $CaCO_3$ peak 'C' with rising temperature.

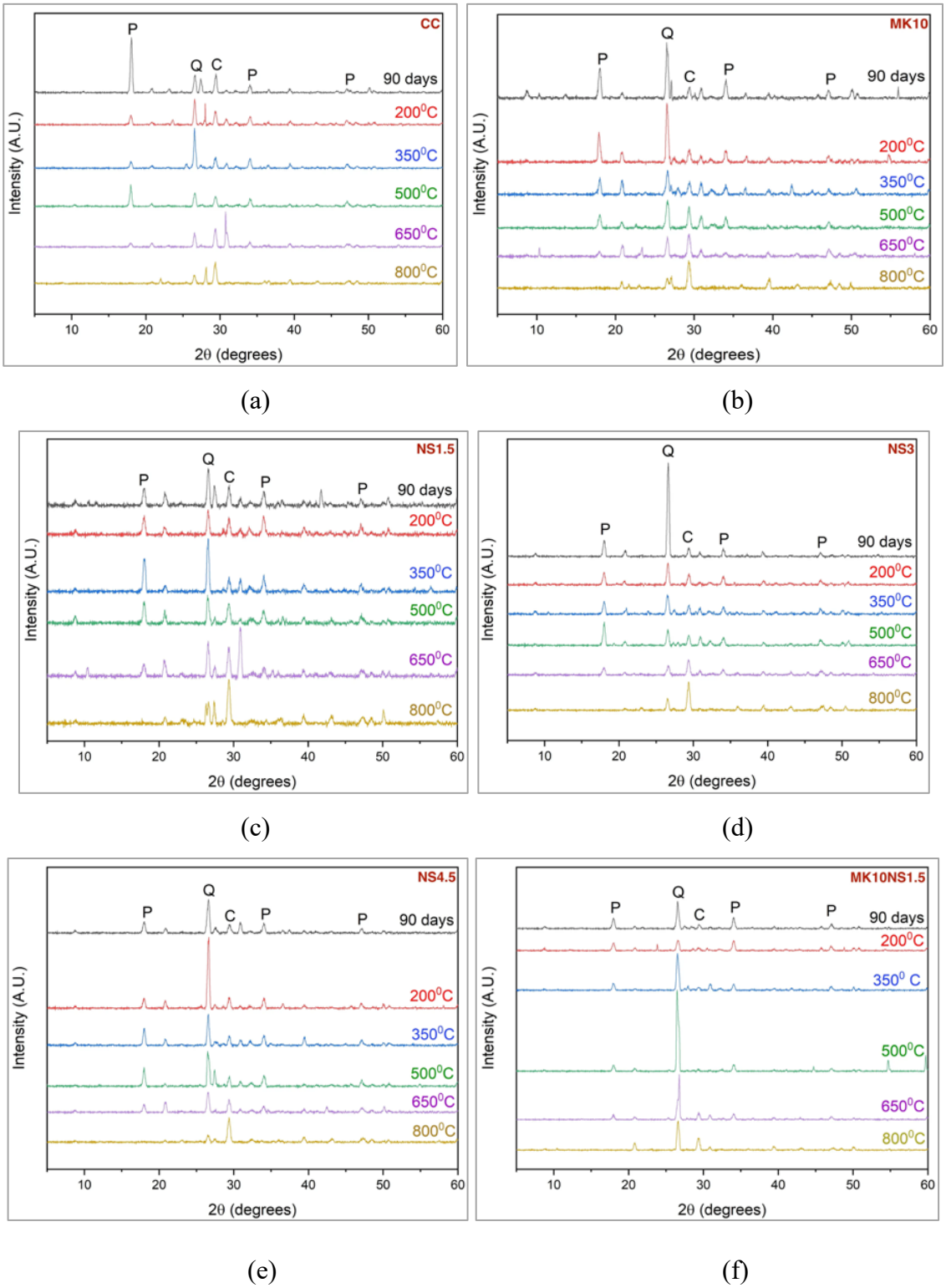

(a) (b)

(c) (d)

(e) (f)

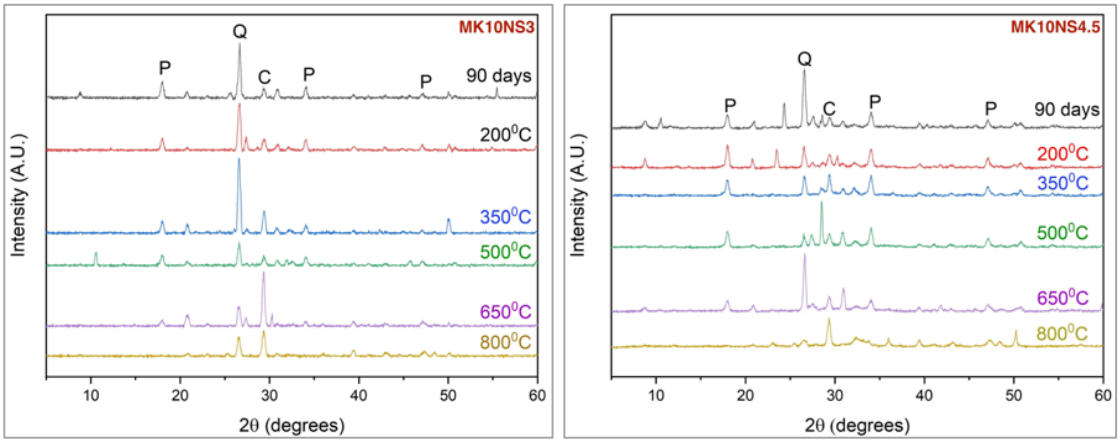

(g) (h)

Figure 6.41. Diffractograms of concrete after exposure at different temperatures

**P – portlandite, Q- quartz, C-calcite*

6.6.2 Thermogravimetric and differential scanning calorimetry (TGA/DSC) analyses

The TGA/DSC curves of the cement and blended cement paste samples at 90 days are shown in Figure 6.42a-h. The mass loss of the samples at different temperature ranges is illustrated in Figure 6.43, and three endothermic peaks were observed: (i) within the range of 30–300 °C, (ii) spanning 400–500 °C, and (iii) extending from 600 to 900 °C. The initial peak, observed between 30°C and 300°C, exhibits a broader mass loss than the subsequent peaks. This phenomenon is primarily attributed to the decomposition of CSH and CAH and associated moisture evaporation. The second endothermic peak, occurring between 400 and 500°C, signifies the decomposition of CH [317]. The third endothermic peak, ranging from 600 to 900°C, corresponds to the loss of water due to the decomposition of CSH and $CaCO_3$ compounds.

Including MK and NS amplifies the mass loss attributable to moisture evaporation, underscoring their high absorption capacity. Notably, a diminished mass loss was

observed in the second peak when MK and NS were introduced, and the lowest peak was observed in MK10NS3 sample. This reduction was linked to the consumption of CH by MK and NS, contributing to enhanced strength. The final peak indicates that optimal replacements result in a decreased amount of $CaCO_3$, particularly in the ternary mix MK10NS3.

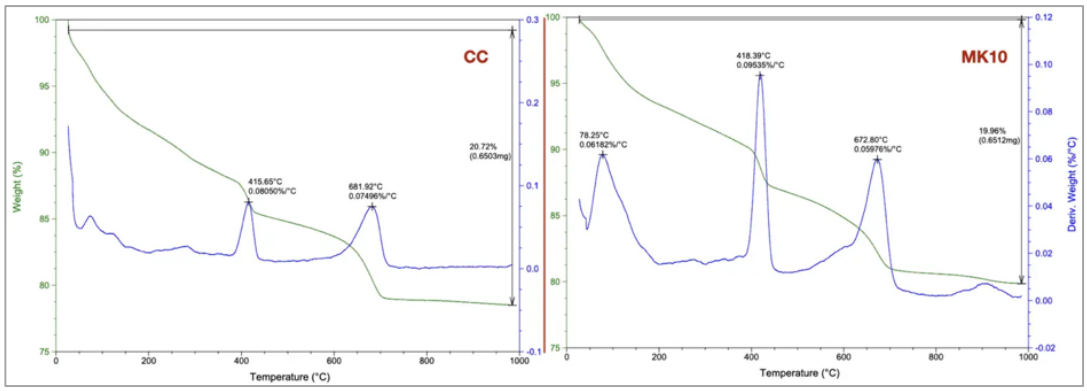

(a)

(b)

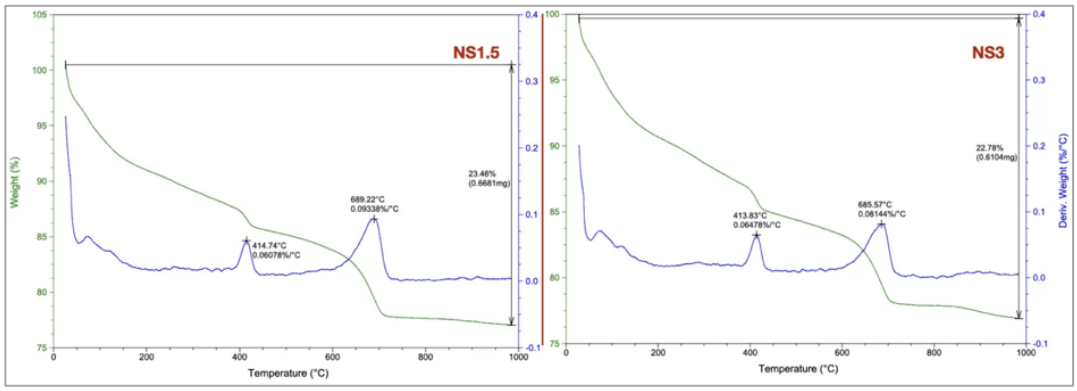

(c)

(d)

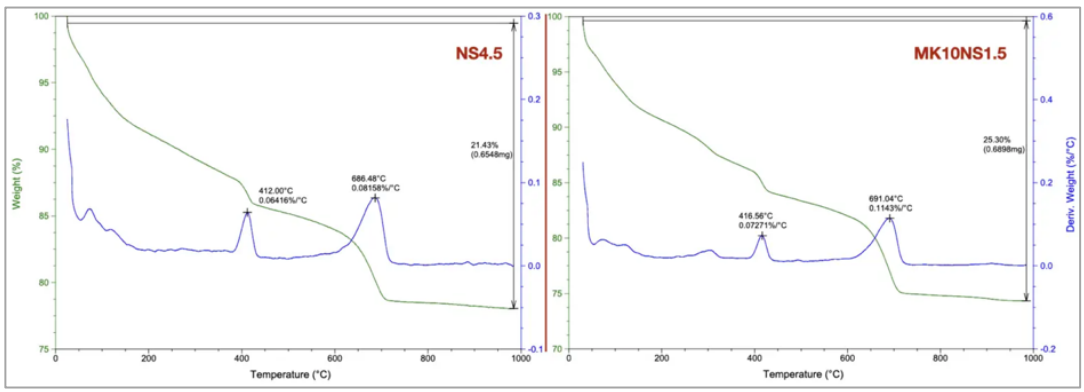

(e)

(f)

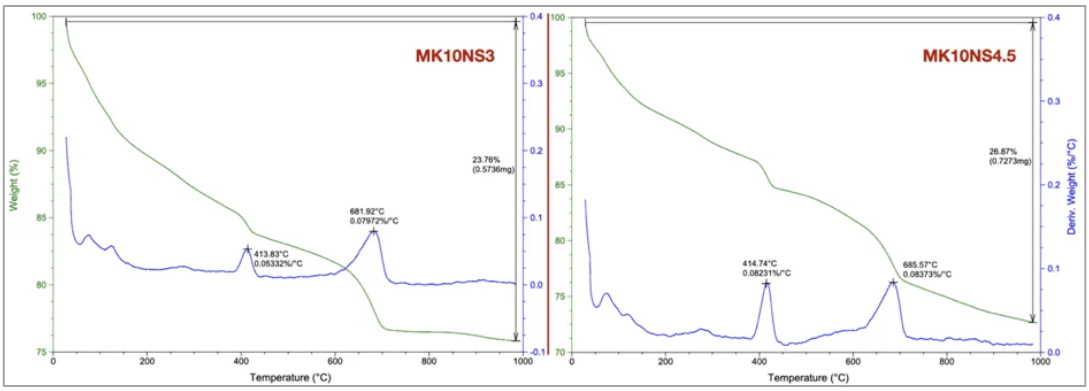

(g) (h)

Figure 6.42 TGA/DSC curves for blended cement pastes cured 90 days

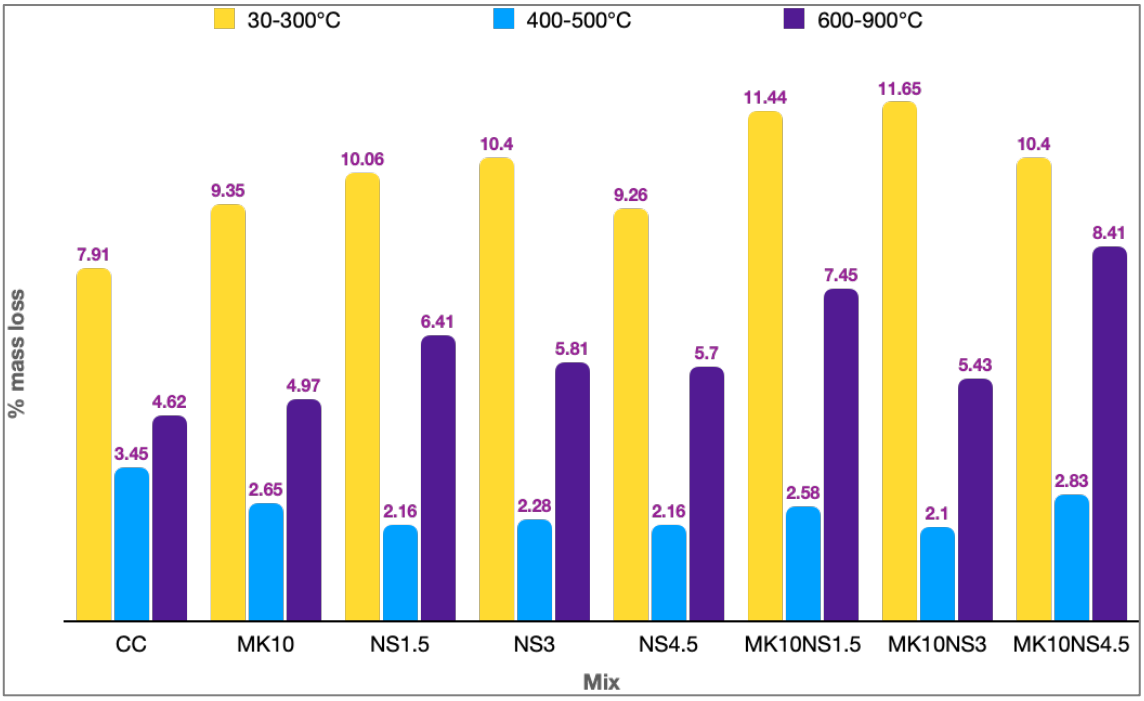

Figure 6.43. TGA/DSC mass loss of different phases of cement/blended cement pastes

6.6.3 Scanning electron microscopic (SEM) analysis

High-resolution scanning electron microscopy (HR-SEM) images unveiled significant morphological transformations in hydration products under elevated temperatures. Following a 90-day curing period at 27±2°C, the samples exhibited a densely packed microstructure with low porosity (Figure 6.44) aligning with the compressive strength observed in the concrete specimens at 90 days (Figure 6.1). Blended cement paste,

particularly in ternary blended samples, displayed a more compacted microstructure attributed to high pozzolanic activity.

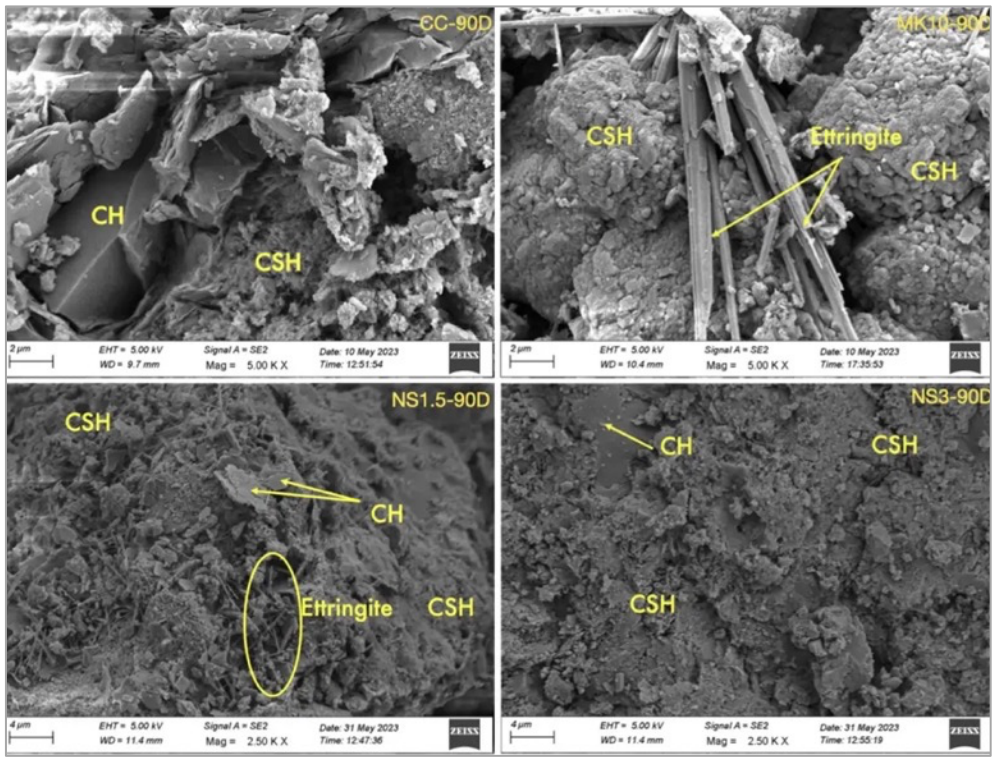

(a)

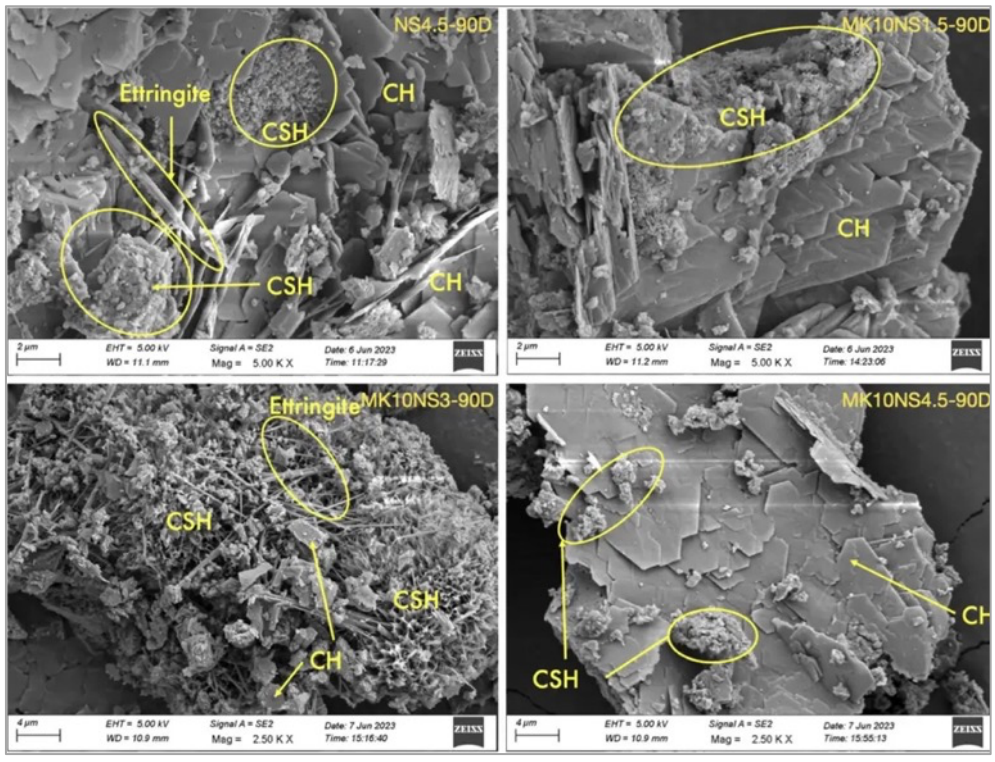

(b)

Figure 6.44 SEM of cement pastes at 90 days

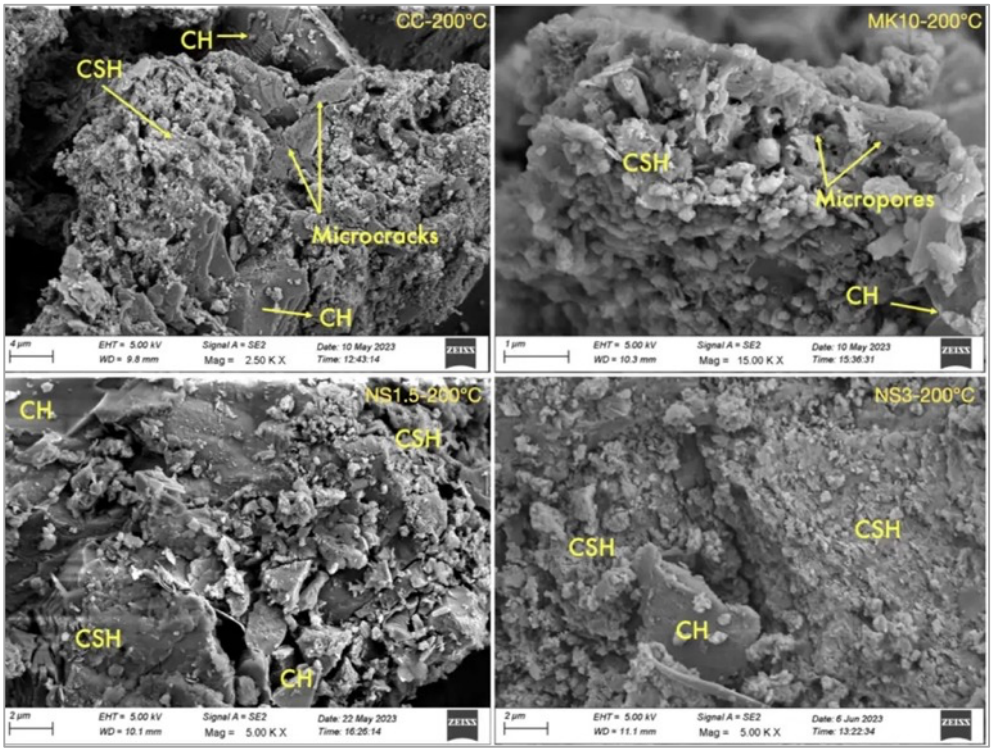

(a)

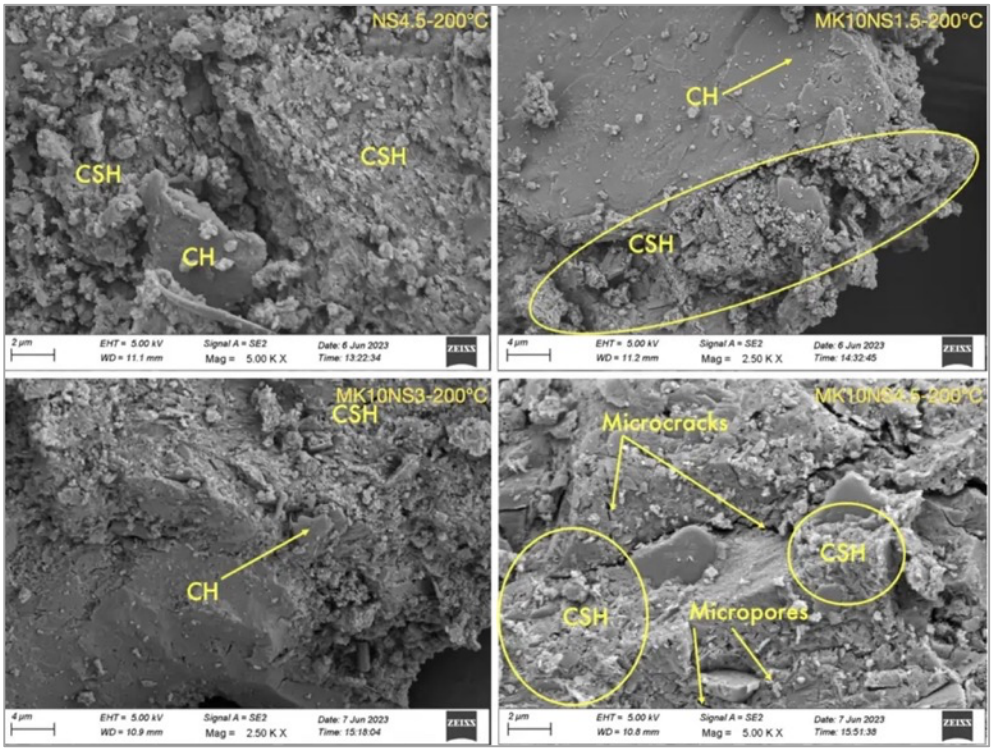

(b)

Figure 6.45 SEM of concrete at 200°C

Upon exposure to temperatures up to 200°C, morphological changes were evident ((b)

Figure 6.45), though not significant, including increased CSH phases due to heightened pozzolanic material reaction with CH. Despite these changes, micropores persisted in the samples, resulting from capillary and adsorbed water evaporation at 200°C [309]. Certain samples, such as the reference and MK10NS1.5, exhibited microcracks, a phenomenon associated with the dehydration of hydration products [318].

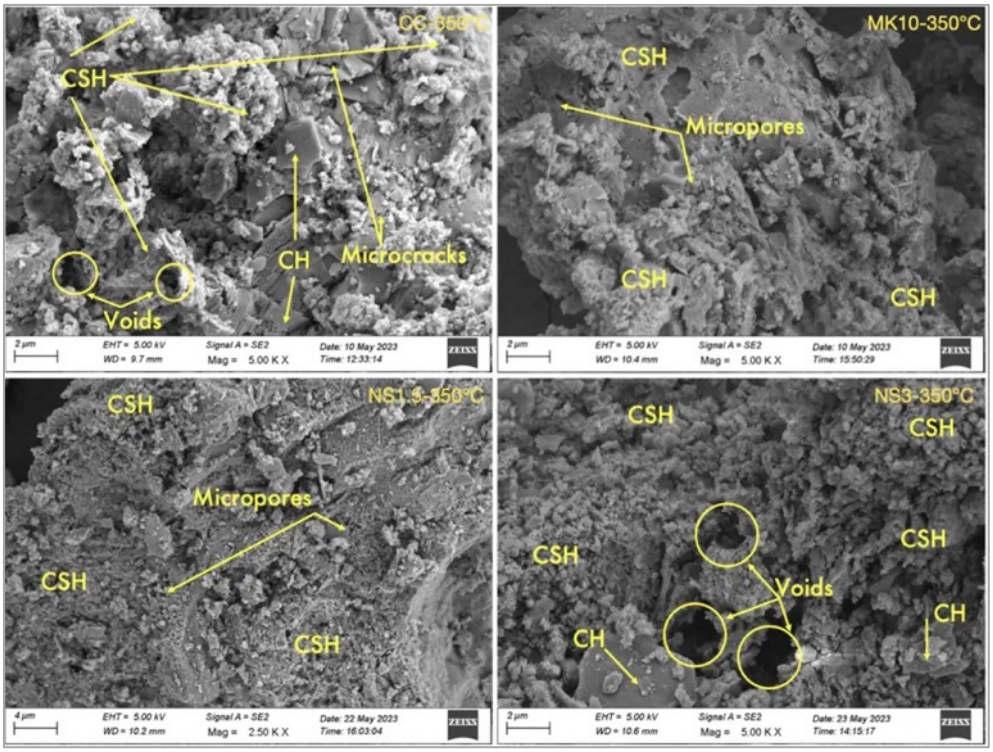

(a)

As the temperature rose to 350°C, the complete evaporation of capillary and adsorbed water ensued, initiating the decomposition of CH. This decomposition, in turn, led to the weakening of the microstructure. Consequently, the microstructure exhibited clearer pores and gaps when contrasted with samples exposed to 200°C, as illustrated in (Figure 6.46). The SEM images revealed a more open matrix of the hydrated phase with discernible voids in samples subjected to 350°C. This observed structural change is a key factor contributing to the decline in compressive strength of the concrete specimens

exposed to this elevated temperature. Notably, the loosening of the matrix and the increased presence of voids played a pivotal role in this reduction in compressive strength.

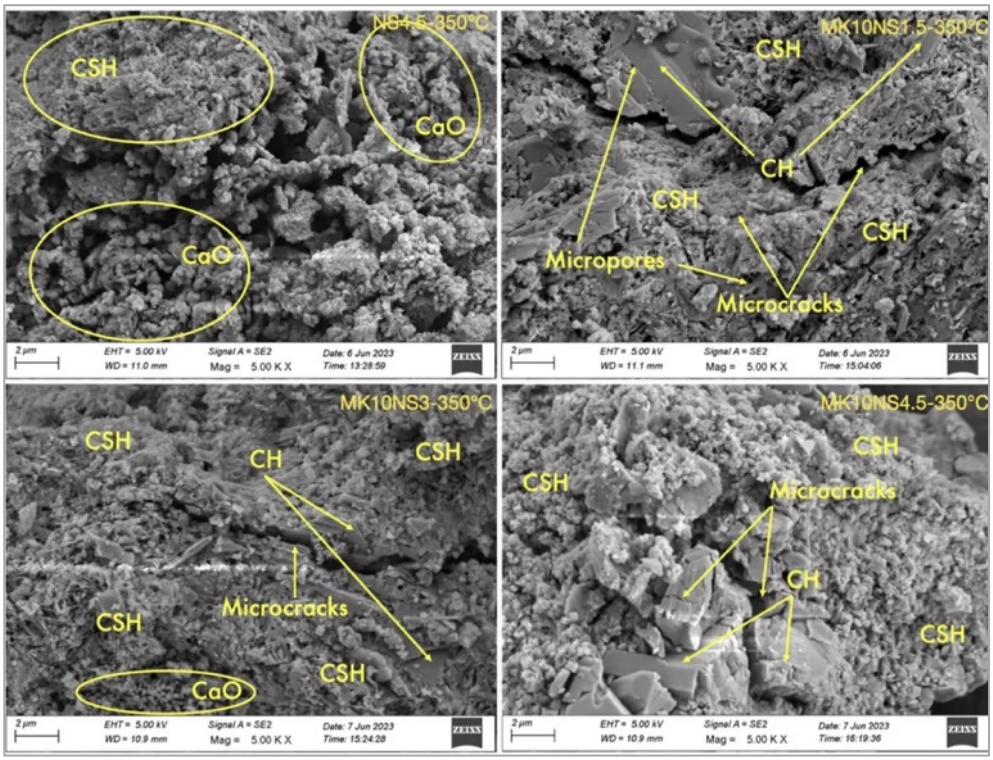

(b)

Figure 6.46 SEM of concrete at 350°C

In line with the findings of Rostasy et al. [319] a discernible increase in the total pore volume with a rise in temperature occurred. However, this pore volume increase was smaller than the substantial increase observed beyond 350°C. This was clear from the morphology of the concrete samples exposed to temperatures above 350°C. This assertion finds support in the analysis of residual compressive strength, where the changes in compressive strength at up to 350°C were modest compared to the significant changes observed within the temperature range of 350°C to 800°C.

As the temperature increased to 500°C, there was a notable escalation in pore coarsening, accompanied by an increased incidence of cracks (Figure 6.47). This phenomenon was

attributed to the breakdown of the partition walls of the pores, as reported by Rostasy et al. in 1980. Despite the microstructure remaining relatively compact at 500°C, the matrix experienced a discernible loosening attributable to the increase in pore size and their increased prevalence compared to conditions at 350°C. An observable shift in the hydrated phases revealed an expansion of pores at 500°C compared to those observed at the lower temperatures. This temperature-induced widening of microcracks and the identification of broader voids were distinct features of the altered microstructure. The presence of CaO in MK10, NS1.5, MK10NS1.5, and MK10NS3 was linked to the CH decomposition reaction at temperatures surpassing 500°C, as highlighted by Hager [311]. Furthermore, the CaO component exhibited a significant expansion of 44% upon cooling to room temperature due to rehydration with ambient humidity, as reported by Hager. This post-cooling rehydration process contributed to the development of additional cracks.

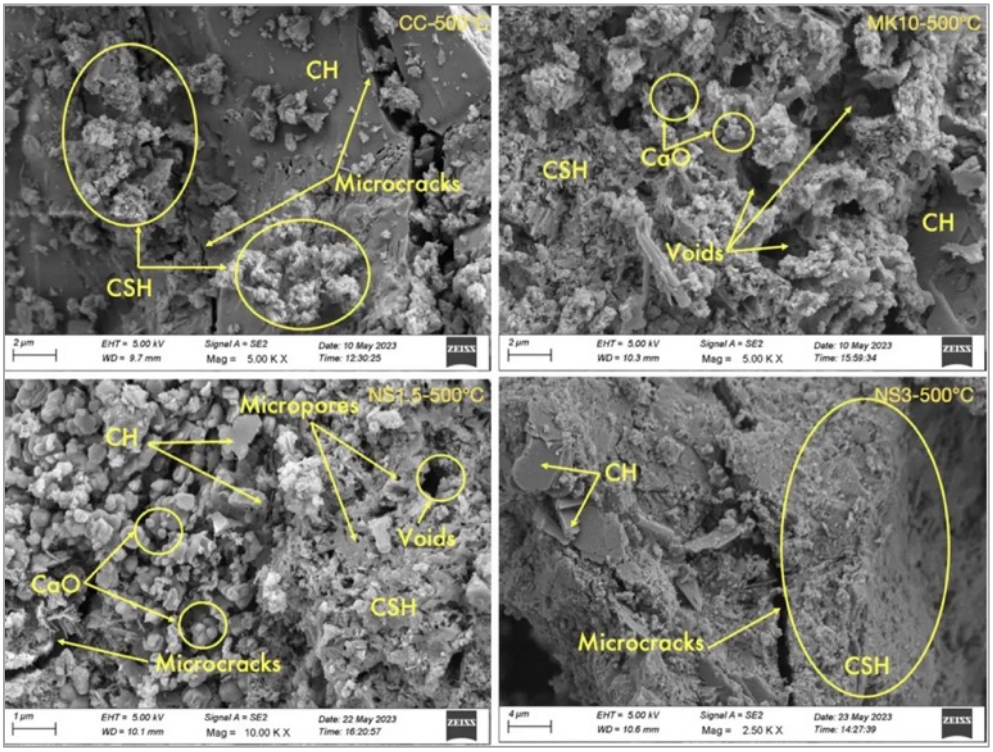

(a)

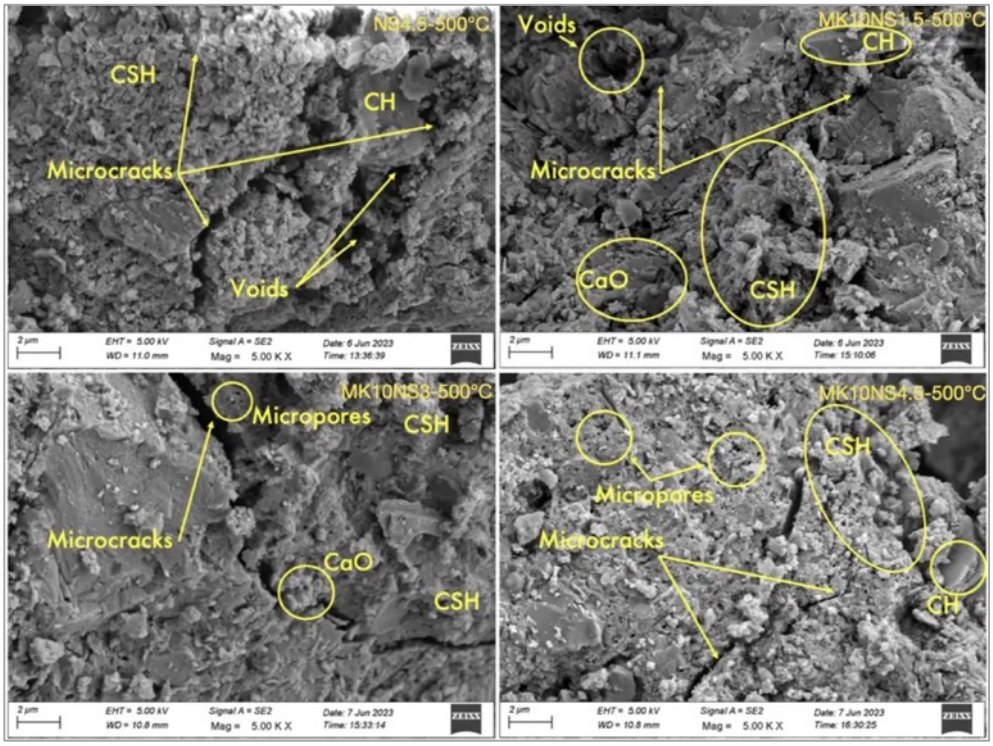

(b)

Figure 6.47 SEM of concrete at 500°C

Upon reaching a temperature of 650°C, most of the hydrated phases underwent decomposition, leading to a fragmented microstructure in the concrete. Examination of the concrete's morphology through SEM (Figure 6.48) revealed increased pores, cracks, and voids. Notably, the thermal exposure resulted in the decomposition of a substantial quantity of CSH gel across all samples, disrupting the naturally dense structure of the gel. The consequential weakening of the concrete microstructure, attributed to the thermal decomposition of the CSH gel, had a detrimental impact on its strength at elevated temperatures. Additionally, the decomposition of a significant amount of CH crystals occurred, forming a granular structure due to volume shrinkage [309].

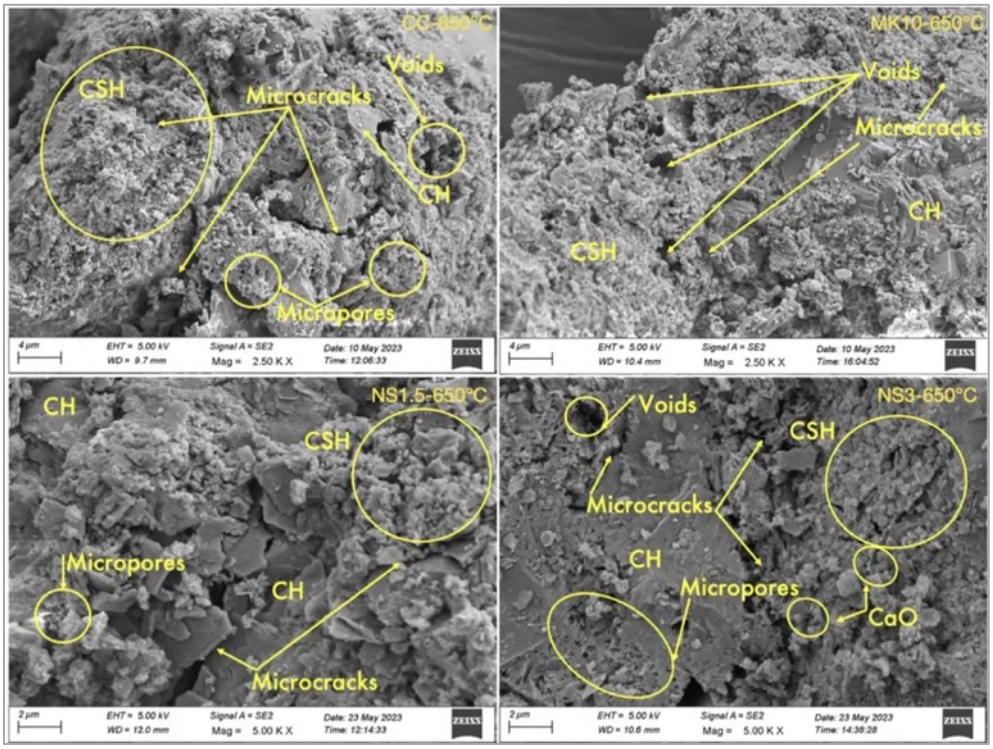

(a)

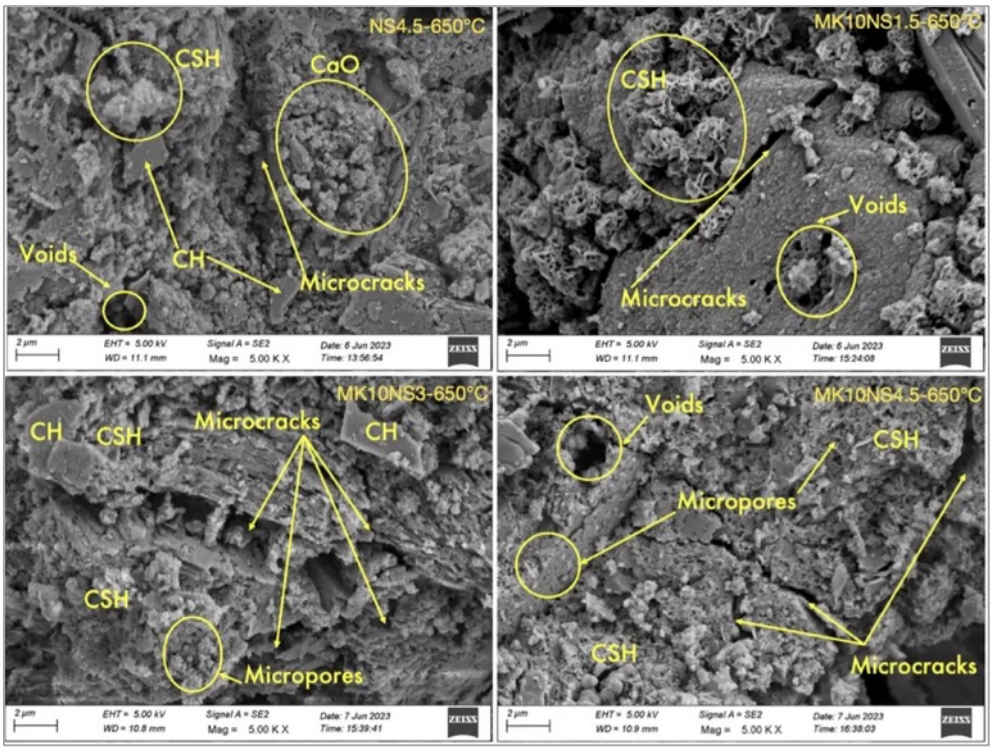

(b)

Figure 6.48. SEM of concrete at 650°C

At a temperature of 800°C, the microstructure of the concrete underwent a pronounced relaxation (Figure 6.49), primarily attributed to the substantial disintegration of hydrates. This disintegration resulted in the loss of their binding force, leading to a notable transformation in the microstructure characterised by an increased prevalence of pores and wider cracks compared to specimens exposed to lower temperatures. The consequence of this alteration was a marked deterioration in the strength of the concrete. An intriguing observation at 800°C was the substantial presence of decomposed CSH gel in the samples. Notably, the conventional understanding is that CSH gel decomposes up to 700°C [320]. The microstructure exhibited several sizable voids across all samples, a manifestation of the breakdown of pore walls. Furthermore, the presence of CaO in the microstructure of NS1.5, NS3, and NS4.5 was identified as a result of CH decomposition.

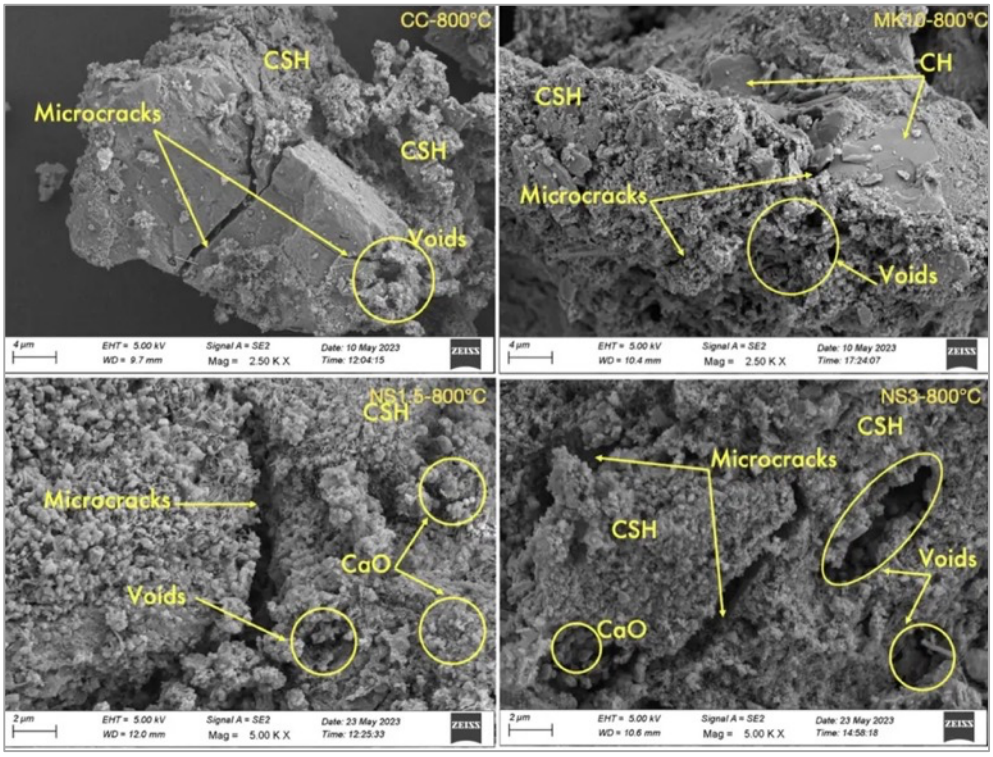

(a)

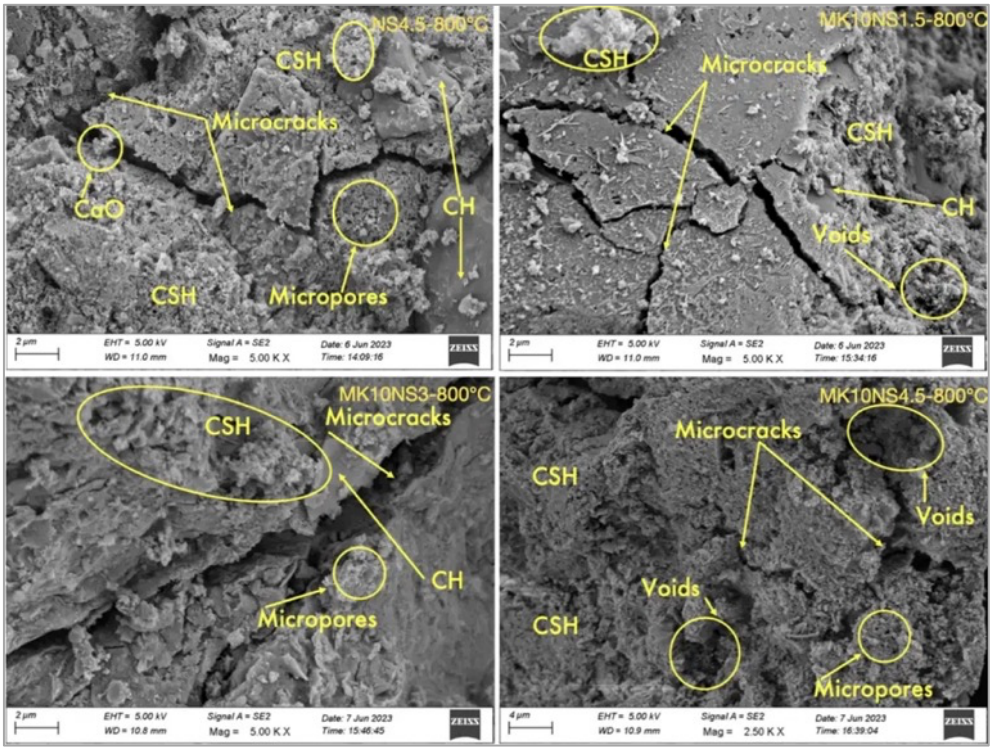

(b)

Figure 6.49 SEM of concrete at 800°C

The HR-SEM analysis revealed significant morphological changes in concrete hydration products under elevated temperatures. After 90 days of curing, the microstructure was densely packed with low porosity. Upon exposure to temperatures up to 200°C, minor morphological changes occurred, including increased CSH phases, while microcracks began to appear at 350°C due to CH decomposition. At 500°C, pore coarsening and microcracks became more prominent. By 650°C, extensive decomposition of CSH gel and CH crystals weakened the microstructure, leading to increased pores and cracks. At 800°C, severe disintegration of hydrates resulted in substantial microstructural relaxation and strength loss

6.7 Summary

In a comprehensive study exploring the compressive strength of binary blends of MK and NS alongside ternary blends, significant advantages over CC were revealed. At the early 3-day stage, MK10 exhibited an 11% strength increase, emphasizing MK's positive impact on early development. Notably, NS3 showcased a remarkable 29% strength increase over CC, and the ternary blend MK10NS3 reached a peak enhancement of 38%, highlighting the synergistic effect. At 28 days, MK10 sustained a 13% strength advantage, NS3 surpassed CC by 21%, and MK10NS3 achieved the highest strength at 69.7 MPa, a 30% improvement over CC. This superior performance extended to 180 days, emphasizing the enduring advantage of ternary blends. Microstructural analyses supported these findings, showcasing the synergistic effects of MK and NS on CSH formation, hydration, and pore structure, contributing significantly to structural engineering.

The study further revealed improvements in split tensile and flexural strengths over different time intervals, with MKNS blends outperforming CC, highlighting the versatility of these blends. Additionally, analyses of carbonation depth, water absorption, and acid resistance underscored the enhanced durability of MKNS blends. The ternary MK10NS3 mix, in particular, demonstrated a remarkable 35% reduction in carbonation depth at 28 days and the lowest mass loss of 5.08% in acid resistance, showcasing its potential for significant improvements in durability. The assessment of thermal stability provided nuanced insights, with MK10 exhibiting superior thermal resistance. The comprehensive analysis of concrete samples subjected to various temperatures, through XRD, TGA/DSC, and SEM, reveals intricate correlations between thermal exposure and concrete performance. XRD analysis indicated that, except for the reference sample, all

mixes displayed an ettringite peak dehydrated between 110°C and 150°C and showed a decline in CH peaks due to decomposition between 400°C and 500°C. This was consistent with the increase in $CaCO_3$ peaks from 400°C onward. TGA/DSC analysis further corroborated these findings, highlighting significant mass loss associated with CH decomposition and moisture evaporation. The introduction of MK and NS reduced mass loss and portlandite peaks, improving strength. SEM images demonstrated that high temperatures led to pronounced microstructural changes, including pore coarsening and increased cracking, particularly beyond 350°C. At 500°C, pore coarsening and crack formation intensified, while at 650°C and 800°C, extensive decomposition of hydration products and significant microstructural relaxation were observed, leading to marked strength deterioration. These findings collectively illustrate how thermal exposure adversely affects concrete microstructure and strength, with MK and NS blends mitigating some effects.